CrossMark

JM PAPERS

Activity-induced propulsion of a vesicle

Zhiwei Peng[1], **Tingtao Zhou**[2] **and John F. Brady**[1,2,†]

[1]Division of Chemistry and Chemical Engineering, California Institute of Technology, Pasadena, CA 91125, USA

[2]Division of Engineering and Applied Science, California Institute of Technology, Pasadena, CA 91125, USA

Modern biomedical applications such as targeted drug delivery require a delivery system capable of enhanced transport beyond that of passive Brownian diffusion. In this work, an osmotic mechanism for the propulsion of a vesicle immersed in a viscous fluid is proposed. By maintaining a steady-state solute gradient inside the vesicle, a seepage flow of the solvent (e.g. water) across the semipermeable membrane is generated, which in turn propels the vesicle. We develop a theoretical model for this vesicle–solute system in which the seepage flow is described by a Darcy flow. Using the reciprocal theorem for Stokes flow, it is shown that the seepage velocity at the exterior surface of the vesicle generates a thrust force that is balanced by the hydrodynamic drag such that there is no net force on the vesicle. We characterize the motility of the vesicle in relation to the concentration distribution of the solute confined inside the vesicle. Any osmotic solute is able to propel the vesicle so long as a concentration gradient is present. In the present work, we propose active Brownian particles (ABPs) as a solute. To maintain a symmetry-breaking concentration gradient, we consider ABPs with spatially varying swim speed, and ABPs with constant properties but under the influence of an orienting field. In particular, it is shown that at high activity, the vesicle velocity is $U \sim [K_\perp/(\eta_e \ell_m)] \int \Pi_0^{swim} \boldsymbol{n} \, d\Omega$, where Π_0^{swim} is the swim pressure just outside the thin accumulation boundary layer on the vesicle interior surface, $\boldsymbol{n}$ is the unit normal vector of the vesicle boundary, $K_\perp$ is the membrane permeability, η_e is the viscosity of the solvent, and ℓ_m is the membrane thickness.

Key words: active matter, colloids, suspensions

† Email address for correspondence: jfbrady@caltech.edu

1. Introduction

Targeted drug delivery is an important goal of modern nanomedicine. Recent advances in the design, manufacture and control of nanocarriers have enabled the delivery of such cargoes into single cells for the purpose of imaging, diagnostics and therapeutics (West & Halas 2003; Gao *et al.* 2005; Rao, Dragulescu-Andrasi & Yao 2007; Torchilin 2012). Commonly used pharmaceutical nanocarriers include liposomes, micelles, nanoemulsions, polymeric nanoparticles and many others (Torchilin 2012). In particular, liposomes have become an important class of carriers for the encapsulation and transport of medical cargoes because of several advantages, including their biocompatibility with human cells, the improved solubility of drugs, and versatility for chemical targeting (Pattni, Chupin & Torchilin 2015), among others.

A liposome is a vesicle that has an aqueous solution core encircled by a hydrophobic membrane (lipid bilayer); hydrophilic solutes dissolved in the core cannot pass readily through the membrane, while lipophilic chemicals tend to associate with the bilayer. As a result, a liposome can be loaded with hydrophilic, lipophilic and/or amphiphilic cargoes in the context of drug delivery. Recently, the Moderna vaccine developed to prevent coronavirus disease 2019 (COVID-19) has utilized a lipid-based nanovesicle to encapsulate the mRNA vaccine that encodes the SARS-CoV-2 spike glycoprotein (Jackson *et al.* 2020).

The liposome-encapsulated medical cargo is transported passively, via either diffusion or advection due to local fluid flow, which limits its ability to overcome biological barriers. To mitigate such limitations of passive drug delivery, active drug delivery platforms using motile microrobots (or microswimmers), either synthetic or biohybrid, have been proposed (Medina-Sánchez, Xu & Schmidt 2018; Erkoc *et al.* 2019; Singh *et al.* 2019; Bunea & Taboryski 2020). By attaching nanoparticle cargoes to the surface of a motile microswimmer, the delivery system can navigate actively, access regions that are unreachable to passive drug delivery, and be directed to the desired site using chemotaxis or an external magnetic field (Felfoul *et al.* 2016; Park *et al.* 2017). Due to self-propulsion of the microswimmer, the effective dispersion of the attached cargo is greatly enhanced, sometimes by a few orders of magnitude, compared to the long-time self-diffusivity of the passively transported cargo (Singh *et al.* 2017).

Instead of attaching a cargo to the surface of a microswimmer, one can also encapsulate both the cargo and the microswimmer inside the vesicle. Encapsulated microswimmers have been studied in previous works. For example, biological microswimmers and self-propelled Janus particles have been encapsulated successfully inside engineered giant unilamellar vesicles (GUVs) (Trantidou *et al.* 2018; Takatori & Sahu 2020; Vutukuri *et al.* 2020). The encapsulated microswimmer provides the vesicle with enhanced super-diffusive motion mediated through hydrodynamic interactions between the microswimmer and the vesicle provided that the fluid is allowed to pass through the membrane of the vesicle (Marshall & Brady 2021).

In the present work, we consider a system that combines the benefits of the vesicle for cargo encapsulation and the self-propulsion of microswimmers for enhanced transport. We propose an alternative model system in which the vesicle is propelled by an osmotic flow that is induced by an actively maintained concentration gradient of a solute inside the vesicle. This kind of osmotic propulsion has been proposed as an alternative mechanism for tumour cells to migrate under strong confinement, in which case other modes of motility, such as contractility, are inhibited. Stroka *et al.* (2014) showed that through physical and biochemical processes, the tumour cell establishes a spatial gradient of solute (ions), which creates a net inflow of water at the cell leading edge and a net outflow at the
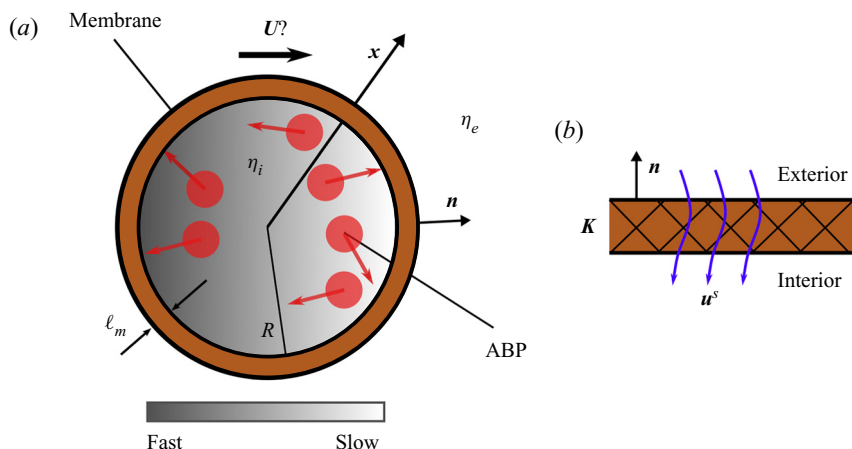
Figure 1. (*a*) A rigid spherical vesicle with a semipermeable membrane immersed in an otherwise quiescent viscous fluid. Active Brownian particles (ABPs) are confined inside the vesicle. (*b*) Schematic of the semipermeable membrane with a permeability tensor $\boldsymbol{K}$ and thickness ℓ_m. The seepage velocity in the membrane is $\boldsymbol{u}^s$, which in general depends on the local position vector.

cell trailing edge. As a result, this water permeation process enables the cell to migrate through narrow channels. We are interested specifically in studying the motility of the vesicle as a result of a prescribed concentration gradient of a solute that is confined inside the vesicle. Because the solute particles are not allowed to pass through the membrane, an osmotic flow of water is generated, which in turn propels the vesicle immersed in water.

The main question that we wish to address in this work is: what is the motility of the vesicle system in relation to the concentration gradient of the solute? More interestingly, does the vesicle move in the same or opposite direction of the concentration gradient?

We show by explicit calculation that for a weakly permeable membrane, the translational velocity of a rigid spherical vesicle becomes

$$U = \frac{1}{4\pi} \frac{K_\perp}{\eta_e \ell_m} \int_{S^2} \Pi_0^{osmo} \boldsymbol{n} \, d\Omega, \tag{1.1}$$

where $\Pi_0^{osmo} = n^w k_B T$ is the osmotic pressure of the solute at the interior wall, n^w is the local number density of the solute in the absence of internal fluid flow, $k_B T$ is the thermal energy, $K_\perp$ is the membrane permeability, η_e is the viscosity of the solvent (water), and ℓ_m is the thickness of the membrane. In (1.1), $\boldsymbol{n}$ is the unit outward normal vector (see figure 1) and the integration is over the solid angle in three dimensions. In this limit, the translational velocity of the vesicle is linearly proportional to the driving force – the osmotic pressure. As expected, a number density at the interior wall that breaks front–back symmetry is required in order to have a non-zero translational velocity of the vesicle.

Equation (1.1) applies generally for any osmotic solute in the weak permeability limit so that the interior fluid flow perturbs the solute distribution only slightly. For example, a linear solute gradient $n_0 = n_0(\mathbf{0}) + \boldsymbol{x} \cdot \nabla n_0$ results in

$$U = \frac{1}{3} \frac{K_\perp}{\eta_e \ell_m} (R - \ell_m) k_B T \, \nabla n_0, \tag{1.2}$$

where ∇n_0 is a constant vector, and R is the exterior radius of the vesicle. Therefore, for the simple prescribed linear-density gradient, the vesicle translates in the same direction as the gradient in number density.

The above discussion reveals that the vesicle is able to exhibit net motion when an interior solute concentration gradient is given. A separate, but important, question is: how can such a solute gradient be maintained? For a biological cell, this is achieved by its internal physical and biochemical processes (Stroka *et al.* 2014). For a synthetic vesicle system for the purpose of enhanced transport, alternative methods need to be implemented in order to generate such a concentration gradient.

In this work, leveraging recent advances in the understanding of the dynamics of active matter, we propose to use active Brownian particles (ABPs) as the solute. In addition to normal thermal Brownian motion with translational diffusivity D_T, ABPs self-propel with an intrinsic 'swim' speed U_s in direction q. The orientation of the swimming direction q changes on a reorientation time scale τ_R that results from either continuous random Brownian rotations or the often-observed discrete tumbling events of bacteria. One important intrinsic length scale due to activity is the run or persistence length $\ell = U_s \tau_R$. Previous works have shown that a spatial variation in the swim speed leads to a spatial variation in the concentration (or number density) of active particles (Schnitzer 1993; Tailleur & Cates 2008; Row & Brady 2020). By tuning the swim speed distribution of ABPs confined inside the vesicle, a spherically asymmetric density distribution can emerge and lead to net motion of the vesicle.

For active particles with slow spatial variation in swim speed in one dimension, Schnitzer (1993) and later Tailleur & Cates (2008) showed that the local number density n is inversely proportional to the local swim speed U_s, i.e. $nU_s = \text{const}$. This simple prediction has been validated experimentally using bacteria that swim with an intensity-dependent speed when illuminated by a spatial light pattern (Arlt *et al.* 2019). Row & Brady (2020) generalized this result and showed that the spatial variation in activity (e.g. swim speed) can be utilized as a pump mechanism in which fluid flows from regions of high concentration of particles to low. Employing this spatial variation, we show that encapsulated ABPs with spatially varying activity can be used to propel the vesicle.

In (1.1) and (1.2), the vesicle velocity appears to be linearly proportional to $k_B T$. However, this does not imply that the driving force is necessarily thermal in origin (in thermodynamic equilibrium no density gradient is present). In the case of ABPs as solute, the active (non-equilibrium) dynamics provides such a density gradient. Analogous to the Stokes–Einstein–Sutherland relation $k_B T = \zeta D_T$, where ζ is the Stokes drag coefficient, an active energy scale $k_s T_s = \zeta \tilde{D}^{swim}$ can be defined for active matter systems (Takatori, Yan & Brady 2014), where $\tilde{D}^{swim} = \tilde{U}_s^2 \tau_R / 6$ is the swim diffusivity. We note that for ABPs with spatially varying swim speed, a characteristic swim speed $\tilde{U}_s$ is used in the definition of the swim diffusivity; the local active energy $k_s T_s(x)$ can also be defined by using the local swim speed $U_s(x)$ and/or local reorientation time $\tau_R(x)$. An important parameter that quantifies the activity of ABPs is the ratio $k_s T_s / (k_B T) = \tilde{D}^{swim} / D_T$. For many active matter systems, this ratio is very large, often exceeding 10^3 (Takatori *et al.* 2016). In this high-activity limit, the ABPs exhibit a thin accumulation boundary layer at the interior surface of the vesicle. As we will show in § 3.2, the local density at the interior wall of the vesicle can be related to the density just outside the boundary layer via the equation $n^w k_B T = n^0 k_s T_s(x) f = \Pi_0^{swim}(x) f$, where Π_0^{swim} is the swim pressure just outside the boundary layer, and f is a factor that depends on the ratio of the run length to the size of the vesicle. (This factor is unity for the case of ABPs on one side of an infinite planar wall; Yan & Brady 2015.) For highly active ($k_s T_s \gg k_B T$) ABPs, (1.1) becomes

$$U = \frac{1}{4\pi} \frac{K_\perp}{\eta_e \ell_m} \int_{S^2} n^0 k_s T_s(x) f n \, d\Omega = \frac{1}{4\pi} \frac{K_\perp}{\eta_e \ell_m} \int_{S^2} \Pi_0^{swim} n f \, d\Omega, \qquad (1.3)$$

showing that the velocity of the vesicle is proportional to the swim pressure. More precisely, it is the variation of the swim pressure (due to the variation in swim speed or run length $\ell(\boldsymbol{x})$) that gives rise to net motion.

Instead of using ABPs with spatially varying swim speed or run length, one can also consider using an external field that orients constant-property ABPs towards a certain direction. External fields such as chemical gradients or magnetic fields can affect the swimming behaviour of microorganisms to facilitate their movement towards a favourable region. In the laboratory, an externally applied magnetic field has been used to guide nanocarriers for the purpose of targeted drug delivery (Pattni *et al.* 2015; Felfoul *et al.* 2016). In the presence of an external orienting field, even for ABPs with constant properties, the front–back symmetry is broken, and net motion of the vesicle is generated. The balance of the strength of the orienting field and the random reorientation due to rotary diffusion is characterized by the Langevin parameter $\chi_R = \Omega_c \tau_R$, where Ω_c is the strength of the angular velocity induced by the field (Takatori & Brady 2014). Noting that the force exerted by the active particles on the wall is $\boldsymbol{F}^w = k_B T \int n^w \boldsymbol{n} \, \mathrm{d}S$ (Yan & Brady 2015), we rewrite (1.1) as $U = K_\perp \boldsymbol{F}^W / (4\pi R^2 \eta_e \ell_m)$. In other words, we need to know the net force that the active particles exert on the wall to determine the net vesicle motion. The force on the wall scales as $N^w \zeta U_s$, where N^w is the total number of particles at the wall, and each particle pushes against the wall with at most its swim force ζU_s. The balance of this force due to the ABPs with the drag force of the porous vesicle moving through an external viscous fluid gives the net motion. Of particular interest is the strong-field limit, where the number of particles on the wall is of the same order as the total number of particles, $N^w / N = O(1)$, and the net speed of the vesicle is the largest, $U \sim K_\perp N \zeta U_s / (R^2 \eta_e \ell_m)$.

This last example, where we argued that the vesicle motion can be deduced from the net swim force of the ABPs balancing the drag of the vesicle, also applies to the so-called 'dry' active matter (Marchetti *et al.* 2013). Dry active matter describes bacteria (or other organisms) that crawl (or even walk) on a surface of a medium of resistivity ζ. Active particles confined to a 'container' that is able to slide along the surface in response to a lateral force will be able to push the container via their 'swim' force if there is an asymmetric distribution of ABPs. The net swim force would scale as $N^w \zeta U_s$, and the container would translate with speed $U_c \sim N^w \zeta U_s / \zeta_c$, where ζ_c is the resistivity for sliding the container along the surface. For dry active matter there is no fluid, thus one does not have the notion of a semipermeable membrane or a seepage velocity driven by an osmotic pressure difference. Nevertheless, the mechanics are the same: like the seepage velocity, the substrate surface must move across the container boundary as it slides along the surface, and the ABPs achieve their propulsive 'crawling' force by pushing off the substrate just like swimmers push off the fluid. Thus at least at high activity, the results derived here apply equally well to dry active matter with an appropriate change in notation.

In the case of a spherical vesicle, its net motion is induced by an asymmetric number density distribution on the vesicle interior surface. An alternative route for the generation of net motion is to use a vesicle with an asymmetric shape. Because the accumulation of ABPs at the interior surface depends on the local curvature of the boundary, a vesicle that has a front–back asymmetry in its shape is able to exhibit net motion. Indeed, the exterior version of the problem, where a passive object is immersed in a bath of active particles, has been studied. It has been shown in experiments and simulations that for an object with shape asymmetry, net motion can be achieved (Sokolov *et al.* 2010; Kaiser *et al.* 2014; Yan & Brady 2018).

To obtain the results for the vesicle motility, in §2 we describe the model and derive a theoretical formulation that governs the dynamics of the vesicle, the interior solute

suspension and the exterior fluid flow. A Darcy-like constitutive law that models the response of the fluid seepage velocity in relation to the fluid stress differences across the membrane is used. This formulation is at the continuum level, where the vesicle is large compared to the size of the ABPs so that the interior (fluid and ABPs) is treated as a suspension; the suspension stress includes the fluid stress and the osmotic pressure of the ABPs. The exterior flow field satisfies the boundary condition that the fluid velocity at the exterior surface of the vesicle consists of the rigid-body motion and a seepage velocity. Because the vesicle is force- and torque-free, we can relate the rigid-body motion to the seepage velocity distribution at the exterior surface using the reciprocal theorem. This approach is similar to treatments of the swimming of microorganisms using the squirmer model (Stone & Samuel 1996), where the boundary velocity at the surface of the swimmer is decomposed into rigid-body motion and the slip velocity distribution.

In situations relevant for the vesicle model considered here, the interior fluid flow is often weak compared to the active self-propulsion. In § 3, by neglecting the interior fluid flow, we show that the total (fluid and osmotic) pressure inside the vesicle is constant, and the leading-order translational velocity of the vesicle is driven by the difference in the fluid pressure across the membrane. As a result, one needs only to compute the distribution of ABPs in the absence of flow, and the resulting number density distribution at the interior wall is used to obtain the translational velocity. The effect of an external orienting field on the dynamics of confined ABPs and the motion of the vesicle is considered in § 3.4. The behaviour of ABPs with slow spatial variation in their swim speed where fluid motion is considered explicitly is discussed in § 4. Finally, we conclude in § 5 with a discussion of the limitations and extensions of this vesicle–ABPs propulsion system.

2. Problem formulation

Consider a rigid vesicle or cell consisting of a thin membrane and a solution core immersed in an otherwise quiescent viscous fluid (see figure 1). The interior of the vesicle is a suspension of potentially active elements, which we model as ABPs. The boundary or membrane of the vesicle is permeable to the solvent (i.e. water) but not to the solute (ABPs). In other words, the membrane is an osmotic membrane and serves as a confining boundary for the ABPs. Relative to the vesicle, the fluid domain is partitioned into interior, exterior and thin porous (in the membrane) regions. The solvent in all regions is identical.

The ABPs encapsulated inside the vesicle swim with a prescribed spatially varying swim speed, which is the driving mechanism for a spatially varying number density.

At small scales relevant to the vesicle–ABPs system proposed here, the inertia of the fluid, the ABPs and the vesicle are negligible. In particular, for motile bacteria such as *E. coli*, which has characteristic size $\sim 1\,\mu$m and swim speed $\sim 30\,\mu$m s^{-1}, the Reynolds number in water is 3×10^{-5}. The resulting speed of the vesicle, and the Reynolds number based on the size of the vesicle and its speed, are also small. In this low-Reynolds-number limit, the dynamics of the fluid is governed by the Stokes equations and there is no external force/torque on the vesicle.

2.1. *The exterior flow*

The exterior domain consists of solvent alone and its dynamics is governed by

$$\nabla \cdot \boldsymbol{\sigma}_f^e = \eta_e \nabla^2 \boldsymbol{u}^e - \nabla p_f^e = \boldsymbol{0}, \quad \nabla \cdot \boldsymbol{u}^e = 0. \tag{2.1a,b}$$

Here, σ_f^e is the stress tensor, η_e is the dynamic viscosity of the solvent, p_f^e is the pressure field, and u^e is the velocity field. Far from the vesicle, the fluid is undisturbed and there is no background flow:

$$p_f^e \to 0 \quad \text{and} \quad u^e \to 0 \quad \text{as } r \to \infty. \tag{2.2a,b}$$

At the exterior surface of the vesicle, we have

$$u^e(x \in S_e) = U + \Omega \times x + u^s(x), \tag{2.3}$$

where S_e denotes the exterior surface of the vesicle, U (Ω) is the rigid-body linear (angular) velocity of the vesicle, and u^s is the local seepage velocity at the exterior surface. The definition of u^s is deferred to § 2.4. We note that (2.3) is similar to the squirmer model where the closely packed cilia tips of a microorganism are modelled as a distribution of radial and tangential velocities on the cell body, often taken to be of spherical shape (Lighthill 1952; Blake 1971).

2.2. *The interior suspension*

The particles and solvent in the interior of the vesicle are treated as a continuum and governed by

$$\nabla \cdot \sigma^i = \eta_i \nabla^2 u^i - \nabla P = 0 \quad \text{and} \quad \nabla \cdot u^i = 0, \tag{2.4a,b}$$

where σ^i is the stress tensor, η_i is the dynamic viscosity of the suspension, and u^i is the velocity field. Here, the total pressure is given by

$$P = p_f^i + nk_BT, \tag{2.5}$$

where p_f^i is the fluid pressure, n is the number density of the ABPs, and k_BT is the thermal energy. In our model, the only contribution to the suspension stress from the ABPs is the osmotic pressure nk_BT.

Here, the swim pressure introduced by Takatori *et al.* (2014) does not enter the analysis directly. Regardless of activity, the particle contribution to the stress is $\sigma_p = -nk_BT I$. In the high-activity limit, however, as shown in (1.3), the vesicle motion results ultimately from the swim pressure variation. Furthermore, we note that additional stress contributions, such as the active hydrodynamic stresslet of ABPs (Saintillan & Shelley 2015), can be incorporated readily into our model. Since the osmotic pressure is present regardless of activity, in this paper we focus on the osmotic pressure and neglect additional stress contributions.

At the interior wall of the vesicle, we have

$$u^i(x \in S_i) = U + \Omega \times x + u^s(x), \tag{2.6}$$

where S_i is the interior surface of the vesicle.

2.3. *Dynamics of ABPs*

The distribution of ABPs confined inside the vesicle is described by the probability density $\Psi(x, q, t)$ as a function of space x, orientation q ($|q| = 1$), and time t. The conservation of

ABPs is governed by the Smoluchowski equation. At steady state, this is given by

$$\nabla \cdot \boldsymbol{j}_T + \nabla_R \cdot \boldsymbol{j}_R = 0, \tag{2.7}$$

where the translational and rotational fluxes are given by, respectively,

$$\boldsymbol{j}_T = \boldsymbol{u}^i \Psi + U_s(\boldsymbol{x})\,\boldsymbol{q}\Psi - D_T\,\nabla\Psi, \tag{2.8}$$

$$\boldsymbol{j}_R = \tfrac{1}{2}\boldsymbol{\omega}^i \Psi - D_R\,\nabla_R\Psi. \tag{2.9}$$

Here, D_T is the thermal diffusivity of ABPs, $\boldsymbol{\omega}^i = \nabla \times \boldsymbol{u}^i$ is the vorticity vector, D_R is the rotary diffusivity, $\nabla_R = \boldsymbol{q} \times \nabla_q$ is the rotary gradient operator, and $U_s(\boldsymbol{x})$ is the intrinsic swim speed of ABPs. The prescribed spatial variation of U_s is the key ingredient of our model, and is responsible for the generation of a concentration gradient of ABPs inside the vesicle.

The conservation of ABPs requires that

$$\int_{V_i} n\,\mathrm{d}\boldsymbol{x} = N, \tag{2.10}$$

where $n = \int \Psi\,\mathrm{d}\boldsymbol{q}$ is the number density, N is the total number of ABPs, and V_i is the volume of the interior of the vesicle. At the interior surface of the vesicle, the flux relative to the rigid-body motion must vanish. This no-flux condition can be written as

$$\boldsymbol{n} \cdot \boldsymbol{j}_T = \boldsymbol{n} \cdot (\boldsymbol{U} + \boldsymbol{\Omega} \times \boldsymbol{x})\,\Psi, \quad \boldsymbol{x} \in S_i, \tag{2.11}$$

where $\boldsymbol{n}$ is the unit normal vector as shown in figure 1. We note that as a model of active elements inside a cell, the rotary diffusivity D_R is biological rather than thermal in origin. As a result, D_R is independent of D_T (which is assumed to be thermal in origin). The rotary diffusivity defines a reorientation time scale $\tau_R = 1/D_R$ that characterizes the relaxation of the swimming direction. The ABPs take a step of magnitude $\ell = U_s\tau_R$, which is often called the run (or persistence) length ℓ, before its swimming direction changes significantly. Note that one might have a reorientation time $\tau_R(\boldsymbol{x})$ that is a function of position in addition to a spatially varying swim speed, as we show below that the important quantity is the run length $\ell(\boldsymbol{x})$.

In contrast to passive Brownian particles, the self-propulsion of active particles introduces a coupling between their rotational and translational dynamics via the swimming motion. That is, even for an isolated active Brownian sphere (which is geometrically isotropic), one must track both its orientation and position. One manifestation of such a coupling is the enhanced long-time self-diffusivity beyond the thermal diffusivity D_T, which for an ABP with constant properties in free space is $D^{eff} = D_T + D^{swim}$, where $D^{swim} = U_s^2\tau_R/6$ (in three dimensions) is the swim diffusivity. In the Smoluchowski equation (2.7), the orientation dynamics is described by the rotational flux – the active particle exhibits rotary Brownian motion and is rotated by the fluid vorticity.

2.4. *Transport in the membrane*

We treat the fluid transport in the membrane using a macroscopic approach similar to Darcy's law; however, the porous region is modelled ultimately as a thin permeable interface. To this end, we first consider the membrane as having a network stress $\boldsymbol{\sigma}^{net}$

and a fluid stress $\boldsymbol{\sigma}_f^m$. The defining characteristic of the semipermeable membrane is that the fluid stress in the membrane balances the seepage velocity (Durlofsky & Brady 1987):

$$\nabla \cdot \boldsymbol{\sigma}_f^m - \eta_e \boldsymbol{R}_m \cdot \boldsymbol{u}^s = \boldsymbol{0}, \tag{2.12}$$

or $\boldsymbol{u}^s = \boldsymbol{K} \cdot \nabla \cdot \boldsymbol{\sigma}_f^m / \eta_e$, where $\boldsymbol{K} = \boldsymbol{R}_m^{-1}$ is the permeability tensor, and $\boldsymbol{R}_m$ is the membrane resistivity. The remaining network stress is responsible for maintaining the osmotic pressure difference across the membrane. That is, we have the force balance on the exterior and interior surfaces, respectively,

$$\boldsymbol{\sigma}_f^e \cdot \boldsymbol{n} = \boldsymbol{\sigma}_f^m \cdot \boldsymbol{n}, \quad \boldsymbol{x} \in S_e, \tag{2.13}$$

$$\boldsymbol{\sigma}_f^i \cdot \boldsymbol{n} = \boldsymbol{\sigma}_f^m \cdot \boldsymbol{n}, \quad \boldsymbol{x} \in S_i. \tag{2.14}$$

Note, importantly, that at the interior surface, $\boldsymbol{\sigma}_f^i$ is the interior fluid stress (it does not contain the osmotic pressure).

We model the membrane as a tangentially isotropic material with the permeability tensor

$$\boldsymbol{K}(\boldsymbol{n}) = K_\perp \boldsymbol{nn} + K_\parallel (\boldsymbol{I} - \boldsymbol{nn}), \tag{2.15}$$

where $K_\perp$ is the normal permeability, and $K_\parallel$ is the tangential one. For a thin membrane, the gradient in (2.12) can be approximated by a finite difference in the normal direction, which after applying the boundary conditions (2.13) and (2.14) leads to

$$\boldsymbol{u}^s(\boldsymbol{n}) = \frac{\boldsymbol{K}}{\eta_e \ell_m} \cdot \left(\boldsymbol{\sigma}_f^e |_{S_e} - \boldsymbol{\sigma}_f^i |_{S_i} \right) \cdot \boldsymbol{n}. \tag{2.16}$$

Here, ℓ_m is the thickness of the membrane, and the thin membrane condition is $\ell_m \ll R$, with R being the radius of the exterior surface. It is understood that in (2.16), $\boldsymbol{u}^s$ is a function of the local outward normal vector $\boldsymbol{n}$ (see figure 1). Equation (2.16) is a linear relation that specifies how a seepage velocity is generated in response to a jump in the fluid stress across the membrane.

In the absence of deviatoric stress, (2.16) reduces to

$$\boldsymbol{u}^s = -\frac{K_\perp}{\eta_e \ell_m} \left(p_f^e |_{S_e} - p_f^i |_{S_i} \right) \boldsymbol{n}, \tag{2.17}$$

which is the more familiar Darcy's law in terms of the fluid pressure difference. In general, the normal flow is driven by the fluid pressure difference as well as the shear stress.

We remark that different boundary conditions across membranes and macroscopic transport equations exist in the literature. For example, an empirical boundary condition was proposed by Beavers & Joseph (1967) and later rationalized by Saffman (1971). This boundary condition was then generalized to a curved surface (Jones 1973). Recently, using multiscale homogenization and matched asymptotic expansions between the near membrane and the far region, Zampogna & Gallaire (2020) developed a macroscopic condition to simulate the interaction between an incompressible fluid flow and a permeable thin membrane. For the purpose of the present work, (2.16) is sufficient.

Because the vesicle is rigid, the preservation of its volume dictates that

$$\int_{S_e} \boldsymbol{u}^s \cdot \boldsymbol{n} \, \mathrm{d}S = 0. \tag{2.18}$$

Henceforth, for simplicity we will assume that the membrane is not permeable in the tangential directions ($K_\parallel = 0$), in which case the seepage velocity is normal to the vesicle surface.

In the above consideration, the vesicle membrane is treated as a rigid and thin porous region. To understand the material response of the vesicle, a proper treatment taking into consideration the constitutive law of the vesicle membrane is needed (Lebedev, Turitsyn & Vergeles 2007; Vlahovska & Gracia 2007). In particular, the bending elasticity and local incompressibility give rise to a surface force density in the membrane, which is balanced by the jump in the traction from the fluid inside and the fluid outside the vesicle membrane. When such effects are included, the shape of the membrane is not known *a priori* and must be determined as part of the solution. If the departure from the spherical shape is small, then a perturbative approach can be adopted for both the membrane dynamics (Lebedev *et al.* 2007; Vlahovska & Gracia 2007) and the fluid mechanics of a nearly spherical particle moving in a viscous fluid (Brenner 1964).

2.5. *Dynamics of the vesicle*

The rigid-body translational and rotational velocities of the vesicle are determined by the force/torque-free conditions given by

$$\int_{S_e} \boldsymbol{\sigma}_f^e \cdot \boldsymbol{n} \, \mathrm{d}S = \boldsymbol{0}, \quad \int_{S_e} \boldsymbol{x} \times \boldsymbol{\sigma}_f^e \cdot \boldsymbol{n} \, \mathrm{d}S = \boldsymbol{0}. \tag{2.19a,b}$$

We can relate the rigid-body velocities U and $\boldsymbol{\Omega}$ to the seepage velocity $\boldsymbol{u}^s$ at the exterior surface using the reciprocal theorem for Stokes flow (Masoud & Stone 2019). The formula for a general body shape is given in Elfring (2015). For the case of a spherical particle, the rigid-body translational and rotational velocities are given by, respectively,

$$U = -\frac{1}{4\pi R^2} \int_{S_e} \boldsymbol{u}^s \, \mathrm{d}S, \quad \boldsymbol{\Omega} = -\frac{3}{8\pi R^3} \int_{S_e} \boldsymbol{n} \times \boldsymbol{u}^s \, \mathrm{d}S. \tag{2.20a,b}$$

In the study of the rigid-body motion of micro-swimmers with prescribed kinematics (gaits), such as squirmers, the reciprocal theorem allows one to bypass the calculation of the unknown flow field, provided that one can solve the resistance/mobility problem for the swimmer shape. For the problem considered here, the seepage velocity of the vesicle is not known *a priori*; we need to determine the rigid-body motion, the exterior/interior flow fields and the distribution of ABPs simultaneously.

2.6. *Non-dimensional equations for a spherical vesicle*

For a spherical vesicle, the angular velocity vanishes ($\boldsymbol{\Omega} = \boldsymbol{0}$) and the torque balance is automatically satisfied. We define a characteristic swim speed $\tilde{U}_s$ such that

$$U_s(\boldsymbol{x}) = \tilde{U}_s \, \hat{U}_s(\boldsymbol{x}). \tag{2.21}$$

For a spatially homogeneous swim speed, $\hat{U}_s(\boldsymbol{x}) = 1$. The average density of ABPs inside the vesicle is $\bar{n} = N/V_i$, where $V_i = 4\pi(R - \ell_m)^3/3$ is the volume of the interior. We use this average density to scale the probability density such that

$$\Psi = \bar{n}g, \tag{2.22}$$

where g is the non-dimensional probability density. To render the governing equations non-dimensional, we scale pressures and stresses by $\bar{n}k_sT_s$, length by R, and fluid/vesicle velocities by $\bar{n}k_sT_sK_\perp/(\eta_e\ell_m)$. Recall that the activity is $k_sT_s = \zeta \tilde{U}_s^2 \tau_R/6$.

Using the characteristic swim speed, we define the swim Péclet number as

$$Pe_s = \frac{\tilde{U}_s \tau_D}{R} = \frac{\tilde{U}_s R}{D_T}, \tag{2.23}$$

which compares the swim speed to the diffusive speed R/τ_D, where $\tau_D = R^2/D_T$ is a diffusive time scale. Another dimensionless parameter for ABPs is defined as

$$\gamma = \sqrt{\frac{\tau_D}{\tau_R}} = \frac{R}{\delta}, \tag{2.24}$$

where $\delta = \sqrt{D_T \tau_R}$ is a microscopic length that quantifies the distance travelled by translational diffusion on the time scale of τ_R. Alternative parameters, including ℓ/δ and ℓ/R, are often used in the literature. These parameters are direct comparisons between different length scales. We note that they are related to Pe_s and γ by $Pe_s = (\ell/\delta)^2(\ell/R)^{-1}$ and $\gamma = (\ell/R)^{-1}\ell/\delta$.

The non-dimensional exterior problem is given by

$$Da\,\nabla^2 \boldsymbol{u}^e = \nabla p_f^e, \tag{2.25}$$

$$\nabla \cdot \boldsymbol{u}^e = 0, \tag{2.26}$$

$$\boldsymbol{u}^e \to \boldsymbol{0} \quad \text{and} \quad p_f^e \to 0 \quad \text{as } r \to \infty, \tag{2.27a,b}$$

$$\boldsymbol{u}^e = \boldsymbol{U} + \boldsymbol{u}^s \quad \text{at } r = 1, \tag{2.28}$$

where

$$Da = \frac{K_\perp}{R\ell_m}, \tag{2.29}$$

is a Darcy number that compares the permeability of the membrane to its characteristic cross-sectional area.

In the interior, the rigid-body translation $\boldsymbol{U}$ has no effect on the fluid dynamics and we need to consider only the deviation $\boldsymbol{u}' = \boldsymbol{u}^i - \boldsymbol{U}$. Thus the non-dimensional flow problem in the interior is governed by

$$\beta\,Da\,\nabla^2 \boldsymbol{u}' = \nabla P, \tag{2.30}$$

$$\nabla \cdot \boldsymbol{u}' = 0, \tag{2.31}$$

$$|\boldsymbol{u}'|, P < \infty \quad \text{at } r = 0, \tag{2.32}$$

$$\boldsymbol{u}' = \boldsymbol{u}^s \quad \text{at } r = \Delta. \tag{2.33}$$

Here,

$$\beta = \frac{\eta_i}{\eta_e} \tag{2.34}$$

is the interior-to-exterior viscosity ratio, and

$$\Delta = \frac{R - \ell_m}{R} \tag{2.35}$$

is the radius ratio between the interior and the exterior surfaces of the membrane. For a thin membrane, $\ell_m/R \ll 1$, Δ is $O(1)$. The non-dimensional total pressure is given by

$$P = p_f^i + \frac{k_B T}{k_s T_s}\,n = p_f^i + \frac{6\gamma^2}{Pe_s^2}\,n, \tag{2.36}$$

where we have used the relation $k_B T/(k_s T_s) = D_T/(\bar{U}_0^2 \tau_R/6) = 6\gamma^2/Pe_s^2$.

The non-dimensional deviatoric stress tensors in the exterior and interior are, respectively,

$$\boldsymbol{\tau}^e = Da\left[\nabla\boldsymbol{u}^e + \left(\nabla\boldsymbol{u}^e\right)^{\mathrm{T}}\right], \quad \boldsymbol{\tau}^i = \beta\,Da\left[\nabla\boldsymbol{u}' + \left(\nabla\boldsymbol{u}'\right)^{\mathrm{T}}\right]. \tag{2.37a,b}$$

The seepage velocity is given by

$$\boldsymbol{u}^s = \boldsymbol{nn}\cdot\left(\boldsymbol{\sigma}_f^e|_{S_e} - \boldsymbol{\sigma}_f^i|_{S_i}\right)\cdot\boldsymbol{n}, \tag{2.38}$$

where $\boldsymbol{\sigma}_f^e = -p_f^e\boldsymbol{I} + \boldsymbol{\tau}^e$ and $\boldsymbol{\sigma}_f^i = -p_f^i\boldsymbol{I} + \boldsymbol{\tau}^i$. The volume conservation of the vesicle is

$$\oint_{S_e}\boldsymbol{u}^s\cdot\boldsymbol{n} = 0. \tag{2.39}$$

The rigid-body translational velocity of the vesicle is then

$$\boldsymbol{U} = -\frac{1}{4\pi}\int_{S^2}\boldsymbol{u}^s\,\mathrm{d}\Omega. \tag{2.40}$$

The non-dimensional Smoluchowski equation and its fluxes, boundary condition and particle conservation are, respectively,

$$\nabla\cdot\boldsymbol{j}_T + \nabla_R\cdot\boldsymbol{j}_R = 0, \tag{2.41}$$

$$\boldsymbol{j}_T = \alpha\,Da\,\boldsymbol{u}'g + Pe_s\,\hat{U}_s(\boldsymbol{x})\,\boldsymbol{q}g - \nabla g, \tag{2.42}$$

$$\boldsymbol{j}_R = \tfrac{1}{2}\alpha\,Da\,\boldsymbol{\omega}'g - \gamma^2\,\nabla_R g, \tag{2.43}$$

$$\boldsymbol{n}\cdot\boldsymbol{j}_T = 0 \quad \text{at } r = \Delta, \tag{2.44}$$

$$\int g\,\mathrm{d}\boldsymbol{q}\,\mathrm{d}\boldsymbol{x} = \frac{4\pi}{3}\Delta^3, \tag{2.45}$$

where we have introduced three non-dimensional parameters, α, Pe_s and γ. The first parameter is a reduced osmotic pressure given by

$$\alpha = \frac{\bar{n}k_sT_s\tau_D}{\eta_e}. \tag{2.46}$$

Physically, this is a comparison between the active driving pressure ($\bar{n}k_sT_s$) and a viscous resistive 'pressure' (η_e/τ_D) on the time scale τ_D.

In the equations above, variables $\{\boldsymbol{u}^e, p_f^e, \boldsymbol{x}, r, \boldsymbol{U}, \boldsymbol{u}^s, P, \boldsymbol{u}'\}$ and gradient operators are non-dimensional even though the same symbols as their dimensional counterparts are used. This is to avoid inconvenience in notation, and henceforth we will work with non-dimensional quantities unless otherwise noted. In table 1, we summarize the independent non-dimensional parameters and their physical implications.

It is convenient to consider the orientational moments of the probability density function. The zeroth-order moment, or the number density, is given by

$$n(\boldsymbol{x}) = \int_{S^2} g\,\mathrm{d}\boldsymbol{q}, \tag{2.47}$$

where S^2 is the surface of the unit sphere in $\mathbb{R}^3$, which represents all possible orientations that $\boldsymbol{q}$ takes. Integrating the Smoluchowski equation over all orientations, we obtain a

Non-dimensional parameter	Mathematical definition	Physical description
α	$\bar{n} k_s T_s \tau_D / \eta_e$	Reduced osmotic pressure
β	η_i / η_e	Viscosity ratio
γ	R / δ	Comparison of R and δ
Da	$K_\perp / (R \ell_m)$	Darcy number
Pe_s	$\tilde{U}_s \tau_D / R$	Swim Péclet number
Δ	$(R - \ell_m) / R$	Radius ratio

Table 1. Independent non-dimensional parameters.

conservation equation for the number density:

$$\boldsymbol{\nabla} \cdot \boldsymbol{j}_n = 0, \tag{2.48a}$$

$$\boldsymbol{j}_n = \alpha \, Da \, \boldsymbol{u}' n + Pe_s \, \hat{U}_s(\boldsymbol{x}) \, \boldsymbol{m} - \boldsymbol{\nabla} n. \tag{2.48b}$$

This equation is coupled to the first moment, or polar order,

$$\boldsymbol{m}(\boldsymbol{x}) = \int_{S^2} \boldsymbol{q} g \, \mathrm{d}\boldsymbol{q}. \tag{2.49}$$

The no-flux condition (2.11) becomes $\boldsymbol{n} \cdot \boldsymbol{j}_n = 0$ for $\boldsymbol{x} \in S_i$. Multiplying the Smoluchowski equation by $\boldsymbol{q}$ and integrating over S^2, we obtain a governing equation for the polar order:

$$\boldsymbol{\nabla} \cdot \boldsymbol{j}_m - \tfrac{1}{2} \alpha \, Da \, \boldsymbol{\omega}^i \times \boldsymbol{m} + 2\gamma^2 \boldsymbol{m} = \boldsymbol{0}, \tag{2.50a}$$

$$\boldsymbol{j}_m = \alpha \, Da \, \boldsymbol{u}' \boldsymbol{m} + Pe_s \, \hat{U}_s(\boldsymbol{x}) \left(\boldsymbol{Q} + \tfrac{1}{3} n \boldsymbol{I} \right) - \boldsymbol{\nabla} \boldsymbol{m}, \tag{2.50b}$$

where

$$\boldsymbol{Q} = \int_{S^2} \left(\boldsymbol{q} \boldsymbol{q} - \tfrac{1}{3} \boldsymbol{I} \right) g \, \mathrm{d}\boldsymbol{q} \tag{2.51}$$

is the trace-free nematic order tensor, and $\boldsymbol{I}$ is the identity tensor of rank 2. The no-flux condition at the interior surface for the polar order becomes $\boldsymbol{n} \cdot \boldsymbol{j}_m = \boldsymbol{0}$. Different from the conservation of the total number of ABPs, the polar order is not conserved, as indicated by the presence of the sink term $2\gamma^2 \boldsymbol{m}$ in (2.50a) even in the absence of flow. This sink term describes the randomization, due to rotary diffusion, of any polar order.

As can be inferred from the above discussion, there is an infinite hierarchical structure to the moment equations. To truncate this infinite set of equations, a closure model such as $\boldsymbol{Q} = \boldsymbol{0}$ is often considered in the literature (Saintillan & Shelley 2015; Yan & Brady 2015). A closure leads to a set of closed equations that can be solved as an approximation to the Smoluchowski equation. We note that a closure approximation is often not uniformly accurate across different regimes of physical parameters or different spatial/time domains, and care must be taken when interpreting results obtained from such methods (Burkholder & Brady 2020; Dulaney & Brady 2020; Peng & Brady 2020). A systematic approach to derive low-order closure models that are able to approximate the full solution of the Smoluchowski equation is still lacking.

In the context of active nematic (apolar) suspensions, the Bingham closure (Chaubal & Leal 1998) has been shown to agree well with the full kinetic theory, and recently, a numerical scheme has been developed to evaluate efficiently the Bingham closure (Weady,

Shelley & Stein 2022). With this closure, simulations with high spatial resolution are performed for active nematics. As note by Weady *et al.* (2022), their closure is formulated for apolar suspensions, and the generalization to polar active matter remains (e.g. ABPs) to be considered. Furthermore, a comparison of the accuracy of different closure models for ABPs is largely unexplored.

The mechanism for an induced concentration gradient from a prescribed activity gradient in the absence of flow has been studied in previous works (Schnitzer 1993; Tailleur & Cates 2008; Row & Brady 2020). To illustrate this mechanism and motivate later discussions, we summarize the simple one-dimensional result here. In the absence of external linear or angular velocities, such as due to flow or orienting field, the governing equation in one dimension for highly active ABPs is $\nabla \cdot (\hat{U}_s \boldsymbol{m}) = 0$, where the diffusive term is neglected. The solution in one dimension is simply $m = 0$. Then (2.50a) reduces to $n\hat{U}_s = \text{const}$. Further, Row & Brady (2020) showed that this spatial variation of activity and concentration can drive a reverse osmotic flow, i.e. fluid flow from regions of high concentration to low. In this work, we exploit this spatial variation to propel a vesicle that is able to maintain an activity gradient in the swim speed of ABPs confined inside.

3. Vesicle motion in the limit of weak interior flow

In many situations, the advection due to the interior fluid flow is much weaker compared to the self-propulsion of the ABPs or its active swim diffusion (small Péclet number), and we may neglect the effect of the fluid velocity disturbance on the distribution of ABPs.

3.1. *Governing equations*

The behaviour of the system in this small-Péclet limit can be derived systematically by considering a weakly permeable membrane, $Da \ll 1$.

If the vesicle is non-permeable ($Da = 0$), then no external or internal flows can be generated, and the vesicle remains stationary despite the non-uniform density distribution and accumulation of the ABPs at the boundary. Due to the scaling of the dimensional velocities by the permeability, the leading-order non-dimensional velocities are $O(1)$ as $Da \to 0$. To study the motion of the vesicle in the $Da \ll 1$ limit, we pose regular expansions for all fields:

$$\boldsymbol{u}^e = \boldsymbol{u}^e_0 + Da \, \boldsymbol{u}^e_1 + \cdots, \tag{3.1}$$

$$p^e_f = p^e_{f,0} + Da \, p^e_{f,1} + \cdots, \tag{3.2}$$

$$\boldsymbol{u}' = \boldsymbol{u}'_0 + Da \, \boldsymbol{u}'_1 + \cdots, \tag{3.3}$$

$$P = P_0 + Da \, P_1 + \cdots, \tag{3.4}$$

$$g = g_0 + Da \, g_1 + \cdots. \tag{3.5}$$

The dimensionless number density is given by $n = \int g \, \mathrm{d}\boldsymbol{q} = n_0 + Da \, n_1 + \cdots$. Similarly, the expansions for the translational and seepage velocities are, respectively,

$$U = U_0 + Da \, U_1 + \cdots, \tag{3.6}$$

$$\boldsymbol{u}^s = \boldsymbol{u}^s_0 + Da \, \boldsymbol{u}^s_1 + \cdots. \tag{3.7}$$

From (2.37a,b), we know that the leading-order deviatoric stresses are $O(Da)$, which does not contribute to the $O(1)$ seepage velocity. As a result, the seepage velocity at leading

order is driven by the fluid pressure difference across the membrane,

$$\boldsymbol{u}_0^s = \left(p_f^i|_{S_i} - p_f^e|_{S_e} \right) \boldsymbol{n}. \tag{3.8}$$

Inserting these expansions into the exterior Stokes equations (2.25) and (2.26) gives, to leading order,

$$\boldsymbol{\nabla} p_{f,0}^e = 0, \quad \boldsymbol{\nabla} \cdot \boldsymbol{u}_0^e = 0. \tag{3.9a,b}$$

The kinematic boundary condition at the exterior surface is $\boldsymbol{u}_0^e(r = 1) = \boldsymbol{U}_0 + \boldsymbol{u}_0^s$. Due to the linearity of Stokes flow, we need only solve (3.9a,b) using the seepage velocity condition ($\boldsymbol{u}_0^e(r = 1) = \boldsymbol{u}_0^s$); the rigid-body translation is determined from the reciprocal theorem given by (2.40). Because $\boldsymbol{u}_0^s$ is in the radial direction, the exterior flow is radial and given by

$$p_{f,0}^e = 0, \quad \boldsymbol{u}_0^e = \frac{\boldsymbol{u}_0^s}{r^2}. \tag{3.10a,b}$$

Similarly, the leading-order equation governing the interior flow is given by

$$\boldsymbol{\nabla} P_0 = 0, \quad \boldsymbol{\nabla} \cdot \boldsymbol{u}_0' = 0. \tag{3.11a,b}$$

At the interior surface, the flow field satisfies the condition $\boldsymbol{u}'(r = \Delta) = \boldsymbol{u}^s$. We note that the interior flow field is not analytically tractable, but it is not required in order to determine the vesicle motion. The total pressure at leading order is a constant, consisting of spatially varying fluid pressure and osmotic pressure:

$$p_{f,0}^i + 6\gamma^2 n_0/Pe_s^2 = P_0 = \text{const.} \tag{3.12}$$

Inserting the expansions into the Smoluchowski equations (2.41)–(2.45), we obtain, at leading order,

$$\boldsymbol{\nabla} \cdot \left(Pe_s \, \hat{U}_s(\boldsymbol{x}) \, \boldsymbol{q} g_0 - \boldsymbol{\nabla} g_0 \right) - \gamma^2 \, \nabla_R^2 g_0 = 0, \tag{3.13}$$

$$\boldsymbol{n} \cdot \left(Pe_s \, \hat{U}_s(\boldsymbol{x}) \, \boldsymbol{q} g_0 - \boldsymbol{\nabla} g_0 \right) = 0 \quad \text{at } r = \Delta, \tag{3.14}$$

$$\int g_0 \, \mathrm{d}\boldsymbol{q} \, \mathrm{d}\boldsymbol{x} = \frac{4\pi}{3} \Delta^3. \tag{3.15}$$

Using (2.40), (3.8) and (3.12), we obtain

$$\boldsymbol{U}_0 = \frac{3\gamma^2}{2\pi \, Pe_s^2} \int_{S^2} n_0(r = \Delta)\boldsymbol{n} \, \mathrm{d}\Omega. \tag{3.16}$$

It is more intuitive to examine the above expression in its dimensional form

$$\boldsymbol{U}_0 = \frac{1}{4\pi} \frac{K_\perp}{\eta_e \ell_m} \int_{S^2} \Pi_0^{osmo}\boldsymbol{n} \, \mathrm{d}\Omega, \tag{3.17}$$

where $\Pi_0^{osmo} = n^w k_B T$ is the dimensional osmotic pressure of ABPs in the absence of flow.

To sum up, one needs to solve (3.13)–(3.15) to obtain the density distribution of ABPs in the absence of flow, and then use (3.16) to calculate the vesicle motion. In the remainder of § 3, the subscript '0' (e.g. g_0, $\boldsymbol{U}_0$) will be dropped for notational convenience.

942 A32-15

In general, one can represent the number density distribution at the spherical interior wall by the complete spherical harmonic expansion

$$n_0(\Delta, \theta, \phi) = \sum_{l=0}^{\infty} \sum_{m=-l}^{m=l} C_{l,m} Y_l^m(\theta, \phi), \quad (3.18)$$

where $Y_l^m = \sqrt{(2l+1)(l-m)!/[4\pi(l+m)!]} P_l^m(\cos\theta) \exp(im\phi)$, and P_l^m is the associated Legendre polynomial of degree l and order m. Using (3.16), a direct integration shows that only the $l = 1$ modes contribute to the translational velocity of the vesicle. This is similar to the tangential spherical squirmer model in which only the 'B_1' mode – the coefficient of $P_1^1(\cos\theta)$ – contributes to the velocity of the squirmer.

3.2. *High activity*

We now explore the limit of high activity, $k_s T_s/(k_B T) = \tilde{D}^{swim}/D_T = \ell^2/(6\delta^2) \gg 1$, which is often observed in active matter systems (Takatori *et al.* 2016). Equivalently, we define $\epsilon = 1/\gamma^2$ (note that $Pe_s = \gamma^2\ell/R$) and consider the limit $\epsilon \to 0$. Expanding the probability density function $g = g^{(0)} + \epsilon g^{(1)} + \cdots$, we obtain, at leading order,

$$\frac{\ell}{R} \nabla \cdot \left[\hat{U}_s \boldsymbol{q} g^{(0)} \right] - \frac{1}{\hat{\tau}_R} \nabla_R^2 g^{(0)} = 0, \quad (3.19)$$

where we have included the spatial variation of $\tau_R(\boldsymbol{x})$ and defined $\tau_R = \tilde{\tau}_R \hat{\tau}_R$, similar to the case of spatially varying swim speed. Integrating over the orientation space leads to an equation for the polar order:

$$\nabla \cdot \left(\hat{U}_s \boldsymbol{m}^{(0)} \right) = 0. \quad (3.20)$$

Equation (3.19) is incompatible with the no-flux boundary condition and thus is valid only in the bulk of the interior. At the interior membrane surface, the swimming flux is balanced by the diffusive flux, which implies the existence of an accumulation boundary layer of thickness $O(\epsilon)$. In this high-activity limit, the number of particles in the boundary layer is still finite, which suggests that the probability density is $O(1/\epsilon)$ as $\epsilon \to 0$. Therefore, the probability density in the boundary layer admits an expansion of the form $g(y, \theta, \phi, \boldsymbol{q}) = g^{(-1)}/\epsilon + g^{(0)} + \cdots$. Defining a stretched boundary-layer coordinate in the radial direction $y = (\Delta - r)/\epsilon$, the Smoluchowski equation, to leading order, is

$$\frac{\ell}{R} \left.\hat{U}_s\right|_{S_i} \boldsymbol{q} \cdot \boldsymbol{e}_r \frac{\partial g^{(-1)}}{\partial y} + \frac{\partial^2 g^{(-1)}}{\partial y^2} = 0, \quad (3.21)$$

$$\frac{\ell}{R} \left.\hat{U}_s\right|_{S_i} \boldsymbol{q} \cdot \boldsymbol{e}_r g^{(-1)} + \frac{\partial g^{(-1)}}{\partial y} = 0 \quad \text{at } y = 0, \quad (3.22)$$

$$g^{(-1)} \to 0 \quad \text{as } y \to +\infty. \quad (3.23)$$

Here, the Taylor expansion $\hat{U}_s(r, \theta, \phi) = \hat{U}_s|_{S_i} - \epsilon y (\mathrm{d}\hat{U}_s/\mathrm{d}r)|_{S_i} + \cdots$ is used. The solution is obtained readily as

$$g^{(-1)} = \begin{cases} A_1(\theta, \phi, \boldsymbol{q}) \exp\left(-\frac{\ell}{R} \hat{U}_s|_{S_i} \boldsymbol{q} \cdot \boldsymbol{e}_r y \right), & \boldsymbol{q} \cdot \boldsymbol{e}_r > 0, \\ 0, & \text{otherwise.} \end{cases} \quad (3.24)$$

This singular accumulation occurs only for particles with orientation pointing towards the wall ($\boldsymbol{q} \cdot \boldsymbol{e}_r > 0$) because otherwise they would swim away. In (3.24), A_1 is an unknown

function that can be determined only from the next-order solution. The boundary-layer solution $g^{(0)}(y, \theta, \phi, \boldsymbol{q})$ in the limit $y \to \infty$ needs to be matched with the solution in the bulk as $r \to \Delta$.

At the interior surface of the vesicle ($y = 0$), the leading-order density is large and given by $\gamma^2 \int_{\boldsymbol{q} \cdot \boldsymbol{e}_r > 0} A_1 \, \mathrm{d}\boldsymbol{q}$. Just outside the boundary layer (i.e. $y \to \infty$), the density is $O(1)$ as $\gamma^2 \to \infty$. This boundary-layer structure allows us to relate the osmotic pressure at the interior surface of the vesicle to the swim pressure outside the boundary layer. To this end, we consider the ratio $n^w k_B T / (n^0 k_s T_s)$, where all quantities are dimensional. The density at the wall n^w and the density outside the boundary layer n^0 are defined locally along the interior surface and are functions of the local surface normal vector $\boldsymbol{n}$. From the above analysis, we have

$$\frac{n^w k_B T}{n^0 k_s T_s} = \frac{\gamma^2 \int_{\boldsymbol{q} \cdot \boldsymbol{e}_r > 0} A_1 \, \mathrm{d}\boldsymbol{q}}{\int g^{(0)}(y \to \infty, \theta, \phi, \boldsymbol{q}) \, \mathrm{d}\boldsymbol{q}} \frac{k_B T}{k_s T_s} = f(\ell/R, \Delta), \qquad (3.25)$$

where $\gamma^2 k_B T / (k_s T_s) = 6R^2/\ell^2$ is not a function of the thermal diffusivity D_T (or ℓ/δ). Because in general A_1 is not tractable analytically, the factor $f(\ell/R, \Delta)$ in the preceding equation cannot be obtained explicitly. Nevertheless, (3.25) reveals the important fact that at high activity,

$$\Pi^{osmo} = n^w k_B T = \Pi_0^{swim} f(\ell/R, \Delta), \qquad (3.26)$$

where $\Pi_0^{swim} = n^0 k_s T_s$. In other words, the osmotic pressure at the wall is equal to the swim pressure in the bulk of the interior just outside the boundary layer, but modified by a scale factor that is a function of ℓ/R and Δ. We emphasize that in (3.26), all quantities are defined locally along the interior surface of the vesicle. This is a generalization of the result of Yan & Brady (2015) for ABPs outside an infinite planar wall, where $n^w k_B T = n^0 k_s T_s$ in the limit $\gamma^2 \to \infty$ because of the absence of curvature of the geometry.

Equation (3.26) allows us to obtain the dimensional speed of the vesicle:

$$U = \frac{1}{4\pi} \frac{K_\perp}{\eta_e \ell_m} \int_{S^2} \Pi_0^{swim} f(\ell/R, \Delta) \, \boldsymbol{n} \, \mathrm{d}\Omega. \qquad (3.27)$$

We note that this relation holds for ABPs with spatially varying swim speed or reorientation time.

To understand the dependence of the motion of the vesicle on ℓ/R, we approach the problem from a micromechanical perspective using Brownian dynamics simulations that resolve the Langevin equations of motion governing the stochastic dynamics of an ABP in its physical and orientation space. The details of the simulation method are given in Appendix A. The ABPs are treated as point particles, and their hard-particle interaction with the vesicle interior boundary is implemented using the potential-free algorithm (Heyes & Melrose 1993). In this approach, the force exerted on the wall due to the collision with ABPs is obtained readily. Consider a simulation of N ABPs that interact only with the boundary independently, but not among themselves. After a time step Δt, some particles might have moved outside the interior wall. For particle i that is now outside, we add a displacement $\Delta \boldsymbol{x}_i$ to the particle such that after the move, the particle is in contact with the boundary. The total force exerted on the wall is then $\boldsymbol{F}^w = -\zeta \sum_{i \in \mathcal{I}} \Delta \boldsymbol{x}_i / \Delta t$, where $\mathcal{I}$ is the set of all particles that are outside the boundary before the hard-sphere move. As seen in (3.17), the net speed of the vesicle is proportional to the net force $\boldsymbol{F}^w$.

In figure 2, we show the dimensionless net force exerted on the interior vesicle surface by the ABPs, $\boldsymbol{F}^w / (4\pi R_i^2 \bar{n} k_s T_s)$, as a function of ℓ/R_i for ABPs with no D_T (infinitely
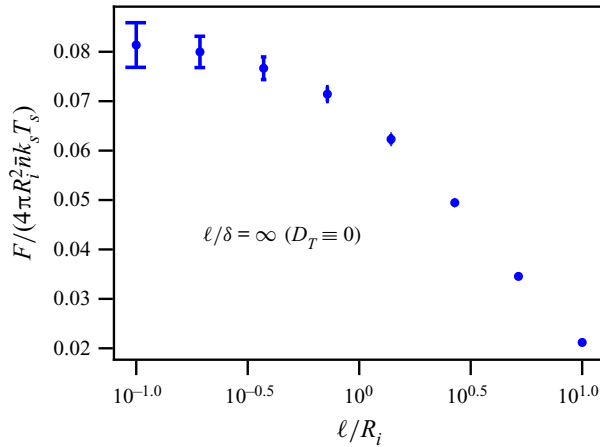
Figure 2. The magnitude of the dimensionless net force on the interior vesicle surface $F^w/(4\pi R_i^2 \bar{n} k_s T_s)$ as a function of ℓ/R_i for ABPs with spatially varying swim speed. The speed profile is a step function where the swim speed in one of the hemispheres is half of that in the other. The reorientation time τ_R is a constant. The net force points towards the side with a higher swim speed.

active, $\ell/\delta = \infty$) and a spatially varying swim speed. The swim speed profile is a step function given by

$$\hat{U}_s = \begin{cases} 1, & x < 0, \\ 1/2, & x > 0. \end{cases} \tag{3.28}$$

The net force points to the side with a larger swim speed, and only the force magnitude is shown in figure 2. As ℓ/R_i increases, the net force decreases. For large ℓ/R_i, the ABPs spend most of their time pushing against and sliding along the interior vesicle surface until rotary Brownian motion reorients them towards the bulk of the interior. In this limit, the number of particles pushing against the interior surface on the side of slow speed is comparable to the side of high speed.

As discussed earlier, in one dimension the relation $nU_s = $ const holds for ABPs with spatially varying properties. In the interior of a vesicle, this relation is still useful for the qualitative understanding of the distribution of ABPs and the motion of the vesicle. Taking the step function given by (3.28) as an example, $n^0 U_s = $ const means that in the bulk of the interior the density on the right side ($x > 0$) is higher than that on the left ($x < 0$), $n_R^0 > n_L^0$. Because $n^w \sim n^0 k_s T_s/(k_B T) \sim n^0 U_s \zeta \ell/(k_B T)$ and $n^0 U_s = $ const, we have $n^w \sim U_s$ for ABPs with constant τ_R. Therefore, the density at the interior vesicle surface on the right side is lower than that on the left ($n_R^w < n_L^w$), which is opposite to the behaviour of the bulk density. Because only the ABPs at the interior surface contribute to the net force, and they can push only against the boundary, this leads to the fact that the net force is in the negative x-direction (to the left). If one had only observations of the number density in the bulk, one would conclude that the vesicle moves in the direction of a lower concentration – a 'reverse' osmotic propulsion (cf. (1.2)).

The number density profile in the bulk and the boundary layer is sketched in figure 3 (red line) for a general swim speed profile that decreases from the left to the right. The variation of the swim speed leads to a gradient in the number density in the bulk of the interior. Two thin accumulation boundary layers are established at the left and right sides of the interior vesicle surface. Because the density at the wall on the right is smaller than that on the left, $n_R^w < n_L^w$, the dimensional version of (3.12) then leads to a larger
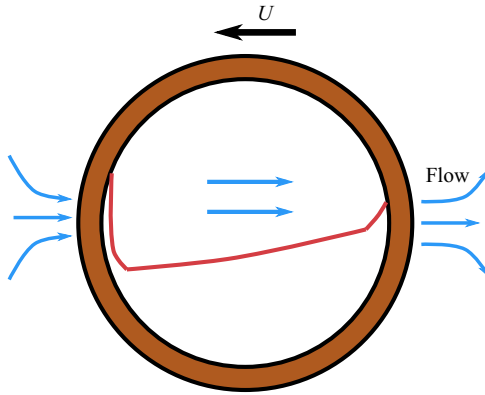
942 A32-18

Figure 3. Schematic of the number density profile (red) and the flow direction (blue) in the high-activity limit for a swim speed profile that decreases from the left to the right. A weak density gradient is present in the bulk of the interior due to the variation of the swim speed. Two accumulation boundary layers are established at the left and right sides of the interior wall, with the density at the wall on the left larger than that on the right. The vesicle–ABPs system as a whole moves by way of jet propulsion.

fluid pressure on the low-density side (right), $p_{f,R}^i > p_{f,L}^i$. Since the fluid pressure in the exterior is homogeneous, the fluid is pushed out of the vesicle from the right and drawn in from the left by conservation of mass. For the vesicle–ABPs system as a whole, it effectively moves by way of jet propulsion. This kind of non-inertial jet propulsion has been proposed and studied in detail by Spagnolie & Lauga (2010) as an alternative mechanism for the locomotion of microswimmers. In their paper, the jetting velocity distribution of a microswimmer (u^s) is prescribed, and then the swim speed is determined from the reciprocal theorem.

Using the approximation $n^0 U_s = \text{const}$ and the relation $\Pi_0^{swim} = n^0 k_s T_s = n^0 U_s \zeta \ell / 6$, we see that it is the variation of run length $\ell(x)$ that is responsible for the net force on the vesicle interior surface and ultimately the vesicle motion. Using (3.27), a Taylor series expansion about the centre of the vesicle leads to the scaling relation $U \sim K_\perp R \zeta n^0 U_s \nabla \ell / (\eta_e \ell_m)$, where $\nabla \ell$ is the gradient of the run length at the centre of the vesicle.

3.3. *A large vesicle*

When the vesicle is large, the confinement is weak, $\ell/R \ll 1$, and ABPs exhibit a thin accumulation boundary layer at the wall and a uniform distribution in the bulk of the interior to leading order. To study this large-vesicle limit of $\ell/R \ll 1$, we first write (3.13) equivalently as

$$\nabla \cdot \left[\frac{\ell}{R} \hat{U}_s(x) \, q g - \left(\frac{\ell}{R} \right)^2 \left(\frac{\ell}{\delta} \right)^{-2} \nabla g \right] - \nabla_R^2 g = 0. \qquad (3.29)$$

In this subsection, we use the definition $\epsilon = \ell/R$ and consider the limit as $\epsilon \to 0$. In the bulk of the interior, we have the expansion $g = g^{(0)} + \epsilon g^{(1)} + \cdots$ and the leading-order equation $\nabla_R^2 g^{(0)} = 0$. The solution in the bulk is then $g^{(0)}(x, q) = n^{(0)}(x)/(4\pi)$. The boundary-layer thickness is determined by a balance between the swimming and diffusive

fluxes, which leads to the leading-order equation

$$-\frac{\partial}{\partial \rho}\left(\frac{\ell}{\delta}\,\hat{U}_s|_{S^i}\,\boldsymbol{q}\cdot\boldsymbol{e}_r g^{(0)} + \frac{\partial}{\partial \rho}g^{(0)}\right) - \nabla_R^2 g^{(0)} = 0, \tag{3.30}$$

$$\frac{\ell}{\delta}\,\hat{U}_s|_{S^i}\,\boldsymbol{q}\cdot\boldsymbol{e}_r g^{(0)} + \frac{\partial}{\partial \rho}g^{(0)} = 0 \quad \text{at } \rho = 0. \tag{3.31}$$

Here, we have used the stretched coordinate $\rho = (\Delta - r)/\epsilon$. Since $\ell \ll R$, curvature of the domain has no effect at $O(1)$, and the boundary-layer equation is similar to that in a planar domain. The $O(1)$ probability density in the boundary layer does not contribute to the $O(1)$ conservation because the boundary-layer thickness is $O(\epsilon)$. This means that the total conservation is given by the density outside the boundary layer alone, $\int n^{(0)}(\boldsymbol{x})\,\mathrm{d}\boldsymbol{x} = 4\pi\Delta^3/3$. In the absence of curvature terms, just like the problem of ABPs on one side of an infinite planar wall (Yan & Brady 2015), the number density at the interior wall of the vesicle at $O(1)$ can be determined analytically; the result is given by

$$\frac{n^w}{n^0} = 1 + \frac{1}{6}\left(\frac{\ell}{\delta}\right)^2 \hat{U}_0^2|_{S^i}. \tag{3.32}$$

In dimensional terms, this means that the osmotic pressure at the wall is $\Pi_0^{osmo} = n^w k_B T = n^0 k_B T + n^0 k_s T_s \hat{U}_s^2$, where n^0 is the density outside the boundary layer. To determine n^0, one needs to solve (3.30) and then match the boundary-layer solution to that in the bulk.

The dimensional translational velocity in the large-vesicle limit is written as

$$\boldsymbol{U} = \frac{1}{4\pi}\frac{K_\perp}{\eta_e \ell_m}\int_{S^2}\left[n^0 k_B T + n^0 k_s T_s\,\hat{U}_s^2|_{S^i}\right]\boldsymbol{n}\,\mathrm{d}\Omega. \tag{3.33}$$

For a large vesicle, the accumulation boundary layer has a structure similar to that obtained in the high-activity limit. Even for weakly active ABPs, this accumulation boundary layer exists so long as $\ell/R \ll 1$. As expected, (3.33) reduces to a form of (3.27) if the activity is high.

3.4. *Vesicle motion due to an external orienting field*

Another way to achieve motion is to apply an external orienting field, which affects the orientational dynamics but not the swim speed of the ABPs. Takatori & Brady (2014) showed that net directed motion of ABPs in free space can be achieved due to the fact that the external field can orient particles to move in the same direction. Instead of having ABPs with spatially varying swim speed, we consider the same orienting field as in Takatori & Brady (2014), but now with ABPs confined inside the vesicle. The only change to the orientational dynamics is that the orienting field exerts an external torque that depends on the orientation of the particle relative to the field direction; the dimensional rotary flux now becomes $\boldsymbol{j}_R = \Omega_c \boldsymbol{q}\times\hat{\boldsymbol{H}}g - D_R\,\nabla_R g$, where Ω_c characterizes the rate of reorientation due to the field, and $\hat{\boldsymbol{H}}$ is the direction of the field. When an ABP is aligned with the field direction ($\boldsymbol{q}\parallel\hat{\boldsymbol{H}}$), the external torque vanishes. The Smoluchowski equation (3.13) for
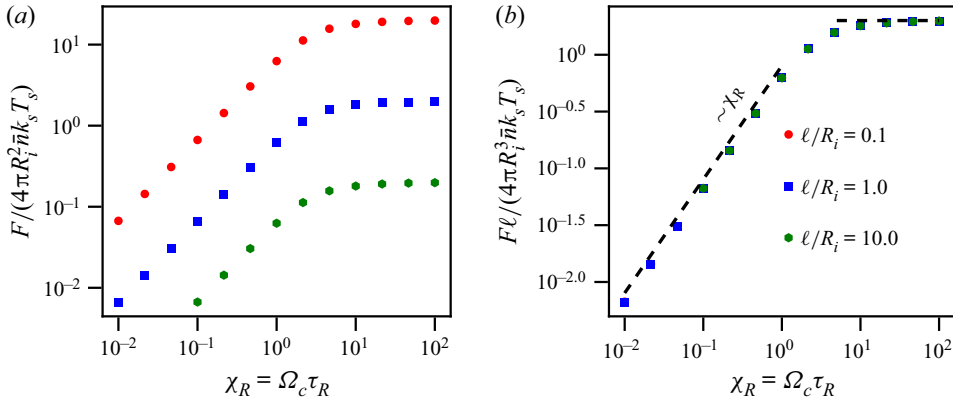
Figure 4. (*a*) The magnitude of the dimensionless net force on the interior wall $F^w/(4\pi R_i^2 \bar{n} k_s T_s)$ as a function of the field strength χ_R for different values of ℓ/R_i. (*b*) The rescaled net force $F^w \ell/(4\pi R_i^3 \bar{n} k_s T_s)$ as a function of χ_R for different values of ℓ/R. All data collapse into one curve in (*b*). The values of ℓ/R_i in both panels are the same and are thus shown only in (*b*). In both panels, the translational diffusion is absent, i.e. $D_T \equiv 0$. In the weak-field limit $\chi_R \ll 1$, the net force is linearly proportional to χ_R, as shown by the dashed line.

ABPs with constant properties in the presence of an orienting field is then

$$\nabla \cdot (Pe_s \, \boldsymbol{q} g - \nabla g) + \gamma^2 \, \nabla_R \cdot \left(\chi_R \boldsymbol{q} \times \hat{\boldsymbol{H}} g - \nabla_R g \right) = 0, \qquad (3.34)$$

while the no-flux boundary condition (3.14) and the total conservation (3.15) remain unchanged. Here, we have defined the Langevin parameter $\chi_R = \Omega_c \tau_R$, which measures the strength of the orienting field compared to rotary diffusion.

In the high-activity limit, an accumulation boundary layer is established at the interior wall. The boundary-layer structure is identical to that obtained for ABPs with spatially varying swim speed. At leading order, the probability density in the bulk of the interior is governed by

$$\frac{\ell}{R} \boldsymbol{q} \cdot \nabla g^{(0)} + \nabla \cdot \left(\chi_R \boldsymbol{q} \times \hat{\boldsymbol{H}} g^{(0)} - \nabla_R g^{(0)} \right) = 0. \qquad (3.35)$$

Compared to (3.19) for spatial variation, the preceding equation has a constant swim speed, and the orientational dynamics is affected by the orienting field. In the boundary layer, the leading-order equation is identical to (3.21), and the density at the wall is large.

Because (3.34) together with its no-flux boundary condition is not analytically tractable, we again make use of Brownian dynamics simulations. In figure 4(*a*), we show the dimensionless net force exerted on the interior wall by the ABPs, $F^w/(4\pi R_i^2 \bar{n} k_s T_s)$, as a function of the field strength for different values of ℓ/R. We note that the net force is in the field direction $\hat{\boldsymbol{H}}$. In figure 4(*b*), the same data are plotted but with the dimensionless net force multiplied by ℓ/R_i. This rescaling allows us to collapse all data onto a single curve. In the linear response regime, the net force is proportional to χ_R. On the other hand, the net force asymptotes to a finite value in the strong-field limit. This is due to the fact that at most all N particles are aligned with $\hat{\boldsymbol{H}}$ and are pushing against the vesicle; further increasing of the field strength beyond this limit has no effect.

In 'wet' active matter systems such as the vesicle problem, the fluid mechanics is ultimately responsible for the motion of the vesicle and needs to be treated properly. Nevertheless, the perspective offered by the dry active matter force balance as discussed in § 1 gives the right answer for the speed of the vesicle. In particular, consider the case in

which the vesicle is driven by an orienting field. The ratio N^w/N is a function of the field strength χ_R, $N^w/N = f(\chi_R)$. As a result, we have the qualitative scaling relation $F^w \sim N\zeta U_s f(\chi_R)$. Noting that $\bar{n} \sim N/R_i^3$ and $k_s T_s \sim \zeta U_s^2 \tau_R$, we have

$$\frac{F^w}{4\pi R_i^2 \bar{n} k_s T_s} \sim \frac{N\zeta U_s}{R_i^2 \bar{n} k_s T_s} f(\chi_R) \sim \frac{R_i}{\ell} f(\chi_R). \tag{3.36}$$

In the weak-field limit, $f(\chi_R) \sim \chi_R$. For large χ_R, $f(\chi_R) \sim 1$ (independent of χ_R). The above scaling argument also explains the collapse of the data as shown in figure 4(*b*). The maximum that F^w may achieve is $N\zeta U_s$, which gives the result that $F^w \ell/(4\pi R_i^3 \bar{n} k_s T_s) = 2$, which is plotted as a horizontal dashed line in figure 4(*b*).

We note that in figure 4, the translational diffusion is absent ($D_T \equiv 0$), which allows the system to achieve the maximum in the net force on the wall. For finite thermal diffusion, the net force is reduced and so is the speed of the vesicle.

4. Slow variation in activity

In the previous section, the dynamics of the vesicle is determined by the distribution of ABPs in the absence of flow. To understand the effect of interior fluid flow on the distribution of ABPs and the dynamics of the vesicle, we consider the case of slow variation in activity. When the activity gradient is small, any smooth variation of the swim speed can be approximated by a Taylor series expansion about the origin. Here, we consider the first effect of a small gradient by keeping the linear term only. The non-dimensional swim speed can be written as

$$\hat{U}_s(\boldsymbol{x}) = 1 + \epsilon \boldsymbol{e} \cdot \boldsymbol{x}, \tag{4.1}$$

where $\epsilon = |\nabla U_s| R/U_s \ll 1$, and $\boldsymbol{e} = \nabla U_s/|\nabla U_s|$ is a constant unit vector in the direction of the gradient. If ϵ is identically zero, then we have a spatially homogeneous swim speed and there is no vesicle motion due to spherical symmetry (see the discussion in § 5). In this case of $\epsilon \equiv 0$, the solution is $\boldsymbol{u}_0' = \boldsymbol{u}_0^e = \boldsymbol{u}_0^s = \boldsymbol{U}_0 = \boldsymbol{0}$, $p_{f,0}^e = 0$ and $P_0 = \text{const}$. The distribution of ABPs is governed by (3.13), (3.14) and (3.15) but with $\hat{U}_s = 1$, i.e. this problem reduces to that of ABPs confined inside a fixed spherical domain. This spherical symmetry means that the number density is a function of the radial coordinate only, $n_0(\boldsymbol{x}) = n_0(r)$. As shown by Yan & Brady (2015), the number density is a monotonically increasing function that obtains its maximum at the interior wall. Because the total pressure P_0 is a constant, this variation of number density (osmotic pressure) maintains a fluid pressure gradient with its maximum at the centre of the interior domain. The fluid pressure across the membrane is constant, and no seepage velocity is generated.

To probe the first effect of a small linear gradient, we pose regular expansions for all fields and the translational velocity:

$$g = g_0 + \epsilon g_1 + \cdots, \tag{4.2}$$

$$\left(P, p_f^e, p_f^i\right) = (P_0, 0, 0) + \epsilon \left(P_1, p_1^e, p_1'\right) + \cdots, \tag{4.3}$$

$$\left(\boldsymbol{u}', \boldsymbol{u}^e, \boldsymbol{u}^s, \boldsymbol{U}\right) = \boldsymbol{0} + \epsilon \left(\boldsymbol{u}_1', \boldsymbol{u}_1^e, \boldsymbol{u}_1^s, \boldsymbol{U}_1\right) + \cdots. \tag{4.4}$$

At $O(\epsilon)$, the exterior fluid and the interior suspension are still governed by (2.25)–(2.28) and (2.30)–(2.33). Similarly, the seepage velocity is related to the jump in the fluid stress

across the membrane given by (2.38). The disturbance to the distribution of ABPs at this order is governed by the inhomogeneous equation

$$\nabla \cdot (Pe_s \, \boldsymbol{q} g_1 - \nabla g_1) - \gamma^2 \, \nabla_R^2 g_1 = -\nabla \cdot \left(\alpha \, Da \, \boldsymbol{u}_1' g_0 + Pe_s \, \boldsymbol{e} \cdot \boldsymbol{x} q g_0 \right)$$
$$- \tfrac{1}{2} \alpha \, Da \, \nabla_R \cdot \left(\boldsymbol{\omega}_1' g_0 \right), \tag{4.5}$$

with the boundary condition

$$\boldsymbol{n} \cdot (Pe_s \, \boldsymbol{q} g_1 - \nabla g_1) = -\alpha \, Da \, \boldsymbol{n} \cdot \boldsymbol{u}_1' g_0 - Pe_s \, \boldsymbol{e} \cdot \boldsymbol{x} \boldsymbol{n} \cdot \boldsymbol{q} g_0 \quad \text{at } r = \Delta. \tag{4.6}$$

The net disturbance is zero, $\int g_1 \, \mathrm{d}\boldsymbol{x} \, \mathrm{d}\boldsymbol{q} = 0$. As can be seen from (4.5), the disturbance fields must be linear to the vector $\boldsymbol{e}$, which allows us to write the number density in the form

$$n_1 = \boldsymbol{e} \cdot \boldsymbol{x} \, h_1(r), \tag{4.7}$$

where $h_1(r)$ is a scalar function of the radial coordinate only.

Due to linearity of the Stokes equations, the interior flow problem at $O(\epsilon)$ admits a solution of the form

$$P_1 = A_1 \boldsymbol{e} \cdot \boldsymbol{x}, \tag{4.8}$$

$$\boldsymbol{u}_1' = A_2 \boldsymbol{e} + A_3 \boldsymbol{e} \cdot \left(\boldsymbol{x}\boldsymbol{x} - \frac{1}{3} r^2 \boldsymbol{I} \right) + \frac{1}{2\beta \, Da} P_1 \boldsymbol{x}. \tag{4.9}$$

Here, the momentum (2.30) is solved using a linear combination of the growing tensor harmonic functions (Leal 2007). The continuity (2.31) gives a constraint

$$5A_3 + \frac{3A_1}{\beta \, Da} = 0. \tag{4.10}$$

We can solve the external flow problem by considering two separate problems with different boundary conditions: (1) $\boldsymbol{u}_1^e = \boldsymbol{u}_1^s$, and (2) $\boldsymbol{u}_1^e = \boldsymbol{U}_1$ at $r = 1$. Instead of solving the flow field due to the second boundary condition in terms of the yet unknown velocity $\boldsymbol{U}_1$, it will be determined from the reciprocal theorem (2.40). As a result, one needs only to compute the exterior flow field due to the seepage velocity $\boldsymbol{u}_1^s$. The exterior flow problem with the first boundary condition has a solution of the form

$$p_1^e = A_4 \boldsymbol{e} \cdot \frac{\boldsymbol{x}}{r^3}, \tag{4.11}$$

$$\boldsymbol{u}_1^e = A_5 \boldsymbol{e} \frac{1}{r} + A_6 \boldsymbol{e} \cdot \left(\frac{\boldsymbol{I}}{r^3} - 3 \frac{\boldsymbol{x}\boldsymbol{x}}{r^5} \right) + \frac{1}{2 \, Da} p_1^e \boldsymbol{x}, \tag{4.12}$$

where the decaying tensor harmonic functions are used. To satisfy the continuity (2.26), we must have

$$A_4 = 2 \, Da \, A_5. \tag{4.13}$$

The seepage velocity connects the interior and exterior flow field via

$$\boldsymbol{u}_1'(\boldsymbol{x} = \Delta \boldsymbol{e}_r) = \boldsymbol{u}_1^s = \boldsymbol{u}_1^e(\boldsymbol{x} = \boldsymbol{e}_r), \tag{4.14}$$

which reduces to

$$A_2 - \frac{1}{3} \Delta^2 A_3 = A_5 + A_6 \quad \text{and} \quad A_3 \Delta^2 + \frac{A_1 \Delta^2}{2\beta \, Da} = -3A_6 + \frac{A_4}{2 \, Da}. \tag{4.15a,b}$$

The volume conservation (2.39) is satisfied. The velocity of the vesicle is obtained from the reciprocal theorem, which gives

$$U_1 = -\frac{1}{4\pi} \int_{S^2} u_1^s \, d\Omega = -\left(A_2 + \frac{A_1 \Delta^2}{6\beta \, Da}\right) e. \qquad (4.16)$$

Finally, to solve (2.38) at this order, we need to compute the fluid stress at the interior and exterior walls. At the interior wall, we have

$$\sigma_{f,1}^i \cdot e_r = -\Delta \left(A_1 - h_1(\Delta) \frac{k_B T}{k_s T_s}\right) e \cdot e_r e_r$$

$$+ \Delta \left(\frac{7}{3} A_3 \beta \, Da + \frac{3}{2} A_1\right) e \cdot e_r e_r + \Delta \left(\frac{1}{3} A_3 \beta \, Da + \frac{1}{2} A_1\right) e. \qquad (4.17)$$

The traction at the exterior wall has two contributions. The first is due to the vesicle translating at a constant speed U_1, which is given by Guazzelli & Morris (2011, p. 44) as

$$\sigma_{U_1}^e \cdot e_r = -\tfrac{3}{2} Da \, U_1. \qquad (4.18)$$

The second contribution is from the seepage velocity boundary condition u_1^s, which is given by

$$-A_4 e \cdot e_r e_r + Da \left(-A_5 - 6A_6 + \frac{A_4}{2\,Da}\right) e + Da \left(-A_5 + 18A_6 - \frac{3A_4}{2\,Da}\right) e \cdot e_r e_r. \qquad (4.19)$$

Using (4.16)–(4.19), we can obtain the jump in the fluid stress across the membrane, which then allows us to calculate the seepage velocity using (2.38). Equating this result with the seepage velocity obtained from (4.12) by setting $r = 1$, we arrive at the following equations for the coefficients:

$$A_5 + A_6 = 0, \qquad (4.20)$$

and

$$\frac{A_4}{2\,Da} - 3A_6 = A_1 \Delta \left(-1 + \frac{\Delta}{4\beta}\right) + \frac{3}{2} Da \, A_2 - \frac{8}{3} A_3 \beta \Delta \, Da - 2A_4$$

$$- 2A_5 \, Da + 12A_6 \, Da - \Delta \, h_1(\Delta) \frac{k_B T}{k_s T_s}. \qquad (4.21)$$

Equation (4.20) implies that u_1^s is proportional to $e \cdot e_r e_r$, and the component proportional to e is zero, which is consistent with the fact that the seepage velocity is in the normal (e_r) direction. At this stage, we have obtained six equations for the six unknown coefficients A_i ($i = 1, \ldots, 6$), which are given by (4.10), (4.13), (4.15a,b), (4.20) and (4.21). Using these equations, one could express A_i in terms of the boundary value of h_1 at the interior wall,

942 A32-24

i.e. $h_1(\Delta)$. These relations are obtained as

$$A_6 = \frac{\Delta^2}{4} \frac{k_B T}{k_s T_s} \frac{h_1(\Delta)}{\Delta + Da\,(6\beta + 4\Delta)} \tag{4.22}$$

and

$$A_1 = \frac{40\,Da\,\beta}{\Delta^2} A_6, \quad A_2 = -8A_6, \quad A_3 = -\frac{24}{\Delta^2} A_6, \tag{4.23a–c}$$

$$A_4 = -2\,Da\,A_6, \quad A_5 = -A_6. \tag{4.24a,b}$$

From (4.16), we have the net motion of the vesicle:

$$U_1 = \frac{4}{3} A_6 e = \frac{\Delta^2}{3} \frac{k_B T}{k_s T_s} \frac{h_1(\Delta)}{\Delta + Da\,(6\beta + 4\Delta)} e. \tag{4.25}$$

Equation (4.25) is the main result of this section. In obtaining (4.25), the only assumption made is the small linear gradient in the swim speed; therefore it applies generally for all ranges of the parameters α, β, Da, Pe_s and γ. In particular, no restriction on the activity of the ABPs (e.g. ℓ/δ) is made. We note that $h_1(\Delta)$ depends parametrically on all the above parameters.

To obtain $h_1(r)$, we need to solve (4.5), which governs the disturbance probability density distribution of the ABPs. As an approximation, we consider the general solution using the $\mathbf{Q} = \mathbf{0}$ closure. At $O(1)$, the spherical symmetry allows us to write the number density and polar order in the forms

$$n_0(\mathbf{x}) = n_0(r), \tag{4.26}$$

$$\mathbf{m}_0(\mathbf{x}) = \mathbf{x} f(r), \tag{4.27}$$

which, when inserted into (2.48*a*) and (2.50*a*), lead to a couple of ordinary differential equations (ODEs) for $n_0(r)$ and $f(r)$. The solutions for n_0 and $\mathbf{m}_0$ under this assumption are obtained by Yan & Brady (2015).

Next, we consider the disturbance distribution of ABPs at $O(\epsilon)$. At this order, the number density distribution is governed by

$$\nabla \cdot \mathbf{j}_{n,1} = 0 \quad \text{and} \quad \mathbf{j}_{n,1} = \alpha\,Da\,\mathbf{u}_1' n_0 + Pe_s\,\mathbf{m}_1 + Pe_s\,\mathbf{e}\cdot\mathbf{x}\mathbf{m}_0 - \nabla n_1. \tag{4.28a,b}$$

The no-flux boundary condition is $\mathbf{n} \cdot \mathbf{j}_{n,1} = 0$ at $r = \Delta$. Similarly, the governing equation for the polar order (assuming $\mathbf{Q}_1 = \mathbf{0}$) is

$$\nabla \cdot \mathbf{j}_{m,1} + 2\gamma^2 \mathbf{m}_1 - \tfrac{1}{2}\alpha\,Da\,\boldsymbol{\omega}_1' \times \mathbf{m}_0 = 0, \tag{4.29}$$

and

$$\mathbf{j}_{m,1} = \alpha\,Da\,\mathbf{u}_1' \mathbf{m}_0 + \tfrac{1}{3} Pe_s\,(n_0 \mathbf{e}\cdot\mathbf{x} + n_1)\,\mathbf{I} - \nabla \mathbf{m}_1. \tag{4.30}$$

No-flux at $r = \Delta$ is $\mathbf{n} \cdot \mathbf{j}_{m,1} = \mathbf{0}$. Similar to (4.7), linearity and symmetry allow us to write the solution to the polar order in the form

$$\mathbf{m}_1 = \mathbf{e}\,h_2(r) + \mathbf{e}\cdot\mathbf{x}\mathbf{x}\,h_3(r), \tag{4.31}$$

where $h_2(r)$ and $h_3(r)$ are functions of the radial coordinate only and satisfy a coupled set of ODEs that can be found in Appendix B.
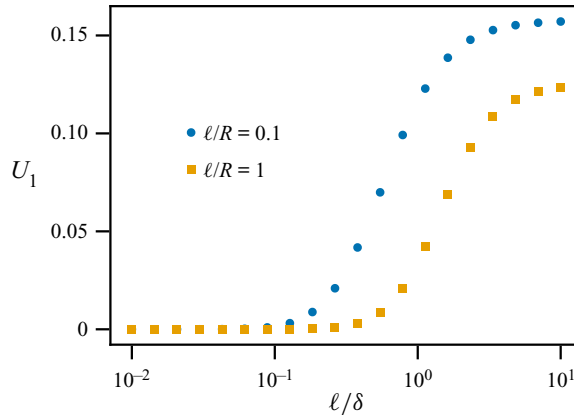
Figure 5. The dimensionless speed of the vesicle U_1 as a function of ℓ/δ for different fixed values of ℓ/R. All other parameters are fixed: $\Delta = 0.98$, $\alpha = 1$, $Da = 0.1$ and $\beta = 1.0$.

In figure 5 we show the dimensionless speed of the vesicle (U_1) as a function of ℓ/δ for $\ell/R = \{0.1, 1\}$. With other dimensionless parameters fixed, the increase of ℓ/δ means the decrease of the translational diffusivity and thus the increase of activity. The speed of the vesicle vanishes as the activity approaches zero, $\ell/\delta \to 0$. As ℓ/δ increases, the speed of the vesicle increases and asymptotes to a finite value for large ℓ/δ. The speed is larger for a smaller ℓ/R because a thin boundary layer near the interior wall develops that enhances the front–back asymmetry of the density distribution.

5. Concluding remarks

In this paper, we have proposed a composite low-Reynolds-number propulsion system made up of active Brownian particles encapsulated in a vesicle for the purpose of enhanced transport beyond that of passive Brownian diffusion. Instead of using the self-propulsion of a microswimmer directly, such as by attaching a cargo to its surface, we considered an alternative mechanism in which the vesicle is propelled by a fluid seepage velocity generated by a concentration gradient of these encapsulated particles. In the present work, we considered the cases in which the concentration gradient is generated by either a prescribed activity gradient in the swim speed of these ABPs or an external orienting field. By tuning the spatial pattern of variation in the swim speed, one could obtain a concentration profile that in turn propels the vesicle with a certain speed or in a desired direction. Alternatively, the application of an external orienting field can push the ABPs against the wall and generate net thrust for the vesicle. We provided a continuum formulation governing the dynamics of the vesicle–ABPs system and analysed its behaviour explicitly in the limits of weak interior flow and small activity gradient. For the composite system as a whole, it moves by jet propulsion at low Reynolds number, i.e. fluid is drawn in from one side of the vesicle and expels from the other. The encapsulation of ABPs only provides a mechanism to generate such a seepage flow.

We emphasize that in the present model, it is the concentration gradient rather than the species of the solute particles that is ultimately responsible for vesicle locomotion. Any osmotic solute, not necessarily active, is able to propel the vesicle so long as a concentration gradient is maintained. For a passive solute, one can maintain a

concentration gradient using chemical reaction, e.g. by placing a distribution of sources and sinks. In this paper, we analysed how such a concentration gradient may be generated by an activity gradient or by the application of an external orienting field. For magnetotactic bacteria or synthetic active particles, an aligning magnetic field can be used to control the direction of the concentration gradient and therefore the direction of motion of the vesicle.

In an experimental setting, a spatial variation of the swim speed of photokinetic bacteria can be achieved by exposing the bacteria to external light intensity gradients. These light-powered bacteria exhibit a larger swim speed in regions of higher light intensity. Under spatially patterned light fields, light-responsive bacteria can self-assemble into reconfigurable structures – 'painting' with bacteria (Arlt *et al.* 2018; Frangipane *et al.* 2018). Another possible mechanism for inducing a spatially varying swim speed could be the spatial modulation of 'fuel' (food sources).

For magnetotactic bacteria, instead of spatial modulation of swim speed, one can use an external static magnetic field that tends to align the bacteria in a certain direction. For static or slowly varying magnetic fields, the magnitude of the induced electric field in this low frequency limit ($\ll 100\,\text{kHz}$) is small so that its effect on the membrane dynamics is negligible (Ye & Curcuru 2015).

In obtaining the results, we assumed that the ABPs can be treated as a continuum and contribute to the suspension stress only via the osmotic pressure. We note that additional constitutive models at the continuum level for the suspension stress can be incorporated readily into our model. The hydrodynamic interactions of the active particles with each other or the confining vesicle boundary are neglected. These effects can be studied using a colloidal approach by considering the detailed interactions among the active particles and with the boundary. For example, this is considered in the study of a single squirmer encapsulated in a porous container by Marshall & Brady (2021), and for the case of a collection of squirmers inside a droplet that is immersed in another fluid by Huang, Omori & Ishikawa (2020).

To achieve net motion of the spherical vesicle, a number density distribution at the vesicle interior wall that breaks the front–back symmetry is required. Instead of maintaining an asymmetric density distribution in a spherical vesicle using ABPs with spatially varying properties or ABPs with constant properties but in an orienting field, one can also consider an asymmetric vesicle. For ABPs with constant properties confined in an asymmetric container, a symmetry-breaking density distribution will emerge because the accumulation of ABPs at the wall depends on the local curvature. The effect of vesicle shape on its net motion is left for a future study.

The enhancement of transport revealed by our study may be useful for the development of synthetic microscale propelling systems for the purpose of delivery of therapeutic payloads, penetrating complex media, or clearing clogged arteries. We hope that our proposed theoretical designs can prompt new experimental implementations.

Declaration of interests. The authors report no conflict of interest.

Author ORCIDs.

Zhiwei Peng https://orcid.org/0000-0002-9486-2837;

Tingtao Zhou https://orcid.org/0000-0002-1766-719X;

John F. Brady https://orcid.org/0000-0001-5817-9128.

Appendix A. Brownian dynamics simulations

The dynamics of ABPs confined inside the vesicle in an external orienting field can be resolved using Brownian dynamics (BD) simulations. Each ABP follows the Langevin equations of motion given by

$$0 = -\zeta(U - U_s q) + F^B + F^w \quad \text{and} \quad 0 = -\zeta_R \Omega + L^B + L^e, \tag{A1a,b}$$

where U (Ω) is the instantaneous linear (angular) velocity, F^B is the Brownian force, F^w is the hard-sphere force due to collisions with the interior wall, ζ_R is the rotary Stokes drag coefficient, L^B is the Brownian torque, and L^e is the external torque due to the field.

The Brownian force and torque satisfy the white noise statistics: $\overline{F^B} = 0$, $\overline{F^B(0) F^B(t)} = 2k_B T \zeta \, \delta(t) \, I$ and $\overline{L^B} = 0$, $\overline{L^B(0) L^B(t)} = 2\zeta_R^2 \, \delta(t) \, I/\tau_R$. Here, $\delta(t)$ is the delta function. In the BD simulations, the particle orientations are represented using unit quaternions. At each time step, the instantaneous particle velocities are computed and then used to update the positions and orientations. The kinematic equation relating the angular velocity and the rate of change of the quaternion is given by Delong, Balboa Usabiaga & Donev (2015).

In figure 4, all data points are obtained by averaging over the long-time behaviour of the system. In each simulation, 10^5 non-interacting ABPs are used, and the system is evolved for a sufficiently long time such that the steady state is reached.

Appendix B. Equations for h_1, h_2 and h_3

In this appendix, we provide the detail on the derivation of the ODEs for h_1, h_2 and h_3. Note that the conservation

$$\int_{|x| \le \Delta} n_1 \, dx = 0 \tag{B1}$$

is satisfied.

Note that

$$\nabla f(r) = x \frac{1}{r} f' \tag{B2}$$

and

$$\nabla (e \cdot x f) = ef + e \cdot xx \frac{1}{r} f'. \tag{B3}$$

Using the identity

$$\nabla \cdot (\underbrace{xx \cdots x}_{k} f(r)) = [(d+k-1)f + rf'] \underbrace{xx \cdots x}_{k-1}, \tag{B4}$$

we can obtain

$$\nabla \cdot [e \cdot xx f(r)] = e \cdot [\nabla \cdot (xx f(r))] = e \cdot x (4f + rf'), \tag{B5}$$

$$\nabla \cdot [e \cdot xxx f(r)] = e \cdot [\nabla \cdot (xxx f(r))] = e \cdot xx (5f + rf'). \tag{B6}$$

Similarly, we have

$$\nabla^2 f = \frac{2}{r} f' + f'', \tag{B7}$$

$$\nabla^2 (\boldsymbol{e} \cdot \boldsymbol{x} f) = \boldsymbol{e} \cdot \boldsymbol{x} \left(\frac{4f'}{r} + f'' \right), \tag{B8}$$

$$\nabla^2 (\boldsymbol{e} \cdot \boldsymbol{xx} f) = 2\boldsymbol{e} f + \boldsymbol{e} \cdot \boldsymbol{xx} \left(\frac{6}{r} f' + f'' \right). \tag{B9}$$

The equation for h_1 is given by

$$\alpha \, Da \, \frac{\mathrm{d} n_0}{\mathrm{d} r} \left(\frac{1}{r} A_2 + \frac{2}{3} r A_3 + \frac{r}{2\beta \, Da} A_1 \right) + Pe_s \left(\frac{1}{r} \frac{\mathrm{d} h_2}{\mathrm{d} r} + 4h_3 + r \frac{\mathrm{d} h_3}{\mathrm{d} r} \right)$$
$$+ Pe_s \left(4f + r \frac{\mathrm{d} f}{\mathrm{d} r} \right) - \frac{4}{r} \frac{\mathrm{d} h_1}{\mathrm{d} r} - \frac{\mathrm{d}^2 h_1}{\mathrm{d} r^2} = 0. \tag{B10}$$

The no-flux condition is given by

$$Pe_s \left(r^2 f + h_2 + r^2 h_3 \right) - h_1 - r \frac{\mathrm{d} h_1}{\mathrm{d} r} + A_2 \alpha \, Da \, n_0 + \frac{\alpha}{6\beta} r^2 n_0 (3A_1 + 4A_3 \, Da \, \beta) = 0, \tag{B11}$$

evaluated at $r = \Delta$. The governing equation for h_2 is

$$\alpha \, Da \left(A_2 - \frac{1}{3} r^2 A_3 \right) f + \frac{1}{3} Pe_s (n_0 + h_1) - \frac{2}{r} \frac{\mathrm{d} h_2}{\mathrm{d} r} - \frac{\mathrm{d}^2 h_2}{\mathrm{d} r^2} - 2h_3$$
$$+ 2\gamma^2 h_2 + \frac{1}{2} \alpha \, Da \left(\frac{5}{3} A_3 + \frac{A_2}{2\beta \, Da} \right) r^2 f = 0. \tag{B12}$$

The no-flux condition at $r = \Delta$ is

$$\frac{\mathrm{d} h_2}{\mathrm{d} r} = 0. \tag{B13}$$

The governing equation for h_3 is

$$\alpha \, Da \left(A_3 + \frac{A_1}{2\beta \, Da} \right) f + \alpha \, Da \, \frac{1}{r} \frac{\mathrm{d} f}{\mathrm{d} r} \left(A_2 + \frac{2}{3} r^2 A_3 + \frac{A_1 r^2}{2\beta \, Da} \right)$$
$$+ \frac{1}{3} Pe_s \frac{1}{r} \left(\frac{\mathrm{d} n_0}{\mathrm{d} r} + \frac{\mathrm{d} h_1}{\mathrm{d} r} \right) - \frac{6}{r} \frac{\mathrm{d} h_3}{\mathrm{d} r} - \frac{\mathrm{d}^2 h_3}{\mathrm{d} r^2}$$
$$+ 2\gamma^2 h_3 - \frac{1}{2} \alpha \, Da \left(\frac{5}{3} A_3 + \frac{A_2}{2\beta \, Da} \right) f = 0. \tag{B14}$$

The no-flux condition is

$$\alpha \, Da \, rf \left(A_2 + \frac{2}{3} r^2 A_3 + \frac{r^2 A_1}{2\beta \, Da} \right) + \frac{1}{3} Pe_s \, r(n_0 + h_1) - 2rh_3 - r^2 \frac{\mathrm{d} h_3}{\mathrm{d} r} = 0, \tag{B15}$$

evaluated at $r = \Delta$. We solve these equations in MATLAB using a Chebyshev collocation method (Trefethen 2000).

REFERENCES

ARLT, J., MARTINEZ, V.A., DAWSON, A., PILIZOTA, T. & POON, W.C.K. 2018 Painting with light-powered bacteria. *Nat. Commun.* **9** (1), 768.

ARLT, J., MARTINEZ, V.A., DAWSON, A., PILIZOTA, T. & POON, W.C.K. 2019 Dynamics-dependent density distribution in active suspensions. *Nat. Commun.* **10** (1), 2321.

BEAVERS, G.S. & JOSEPH, D.D. 1967 Boundary conditions at a naturally permeable wall. *J. Fluid Mech.* **30** (1), 197–207.

BLAKE, J.R. 1971 A spherical envelope approach to ciliary propulsion. *J. Fluid Mech.* **46** (1), 199–208.

BRENNER, H. 1964 The Stokes resistance of a slightly deformed sphere. *Chem. Engng Sci.* **19** (8), 519–539.

BUNEA, A.-I. & TABORYSKI, R. 2020 Recent advances in microswimmers for biomedical applications. *Micromachines* **11** (12), 1048.

BURKHOLDER, E.W. & BRADY, J.F. 2020 Nonlinear microrheology of active Brownian suspensions. *Soft Matt.* **16**, 1034–1046.

CHAUBAL, C.V. & LEAL, L.G. 1998 A closure approximation for liquid-crystalline polymer models based on parametric density estimation. *J. Rheol.* **42** (1), 177–201.

DELONG, S., BALBOA USABIAGA, F. & DONEV, A. 2015 Brownian dynamics of confined rigid bodies. *J. Chem. Phys.* **143** (14), 144107.

DULANEY, A.R. & BRADY, J.F. 2020 Waves in active matter: the transition from ballistic to diffusive behavior. *Phys. Rev.* E **101**, 052609.

DURLOFSKY, L. & BRADY, J.F. 1987 Analysis of the Brinkman equation as a model for flow in porous media. *Phys. Fluids* **30** (11), 3329–3341.

ELFRING, G.J. 2015 A note on the reciprocal theorem for the swimming of simple bodies. *Phys. Fluids* **27** (2), 023101.

ERKOC, P., YASA, I.C., CEYLAN, H., YASA, O., ALAPAN, Y. & SITTI, M. 2019 Mobile microrobots for active therapeutic delivery. *Adv. Ther.* **2** (1), 1800064.

FELFOUL, O., *et al.* 2016 Magneto-aerotactic bacteria deliver drug-containing nanoliposomes to tumour hypoxic regions. *Nat. Nanotechnol.* **11** (11), 941–947.

FRANGIPANE, G., DELL'ARCIPRETE, D., PETRACCHINI, S., MAGGI, C., SAGLIMBENI, F., BIANCHI, S., VIZSNYICZAI, G., BERNARDINI, M.L. & DI LEONARDO, R. 2018 Dynamic density shaping of photokinetic *E. coli. eLife* **7**, e36608.

GAO, X., YANG, L., PETROS, J.A., MARSHALL, F.F., SIMONS, J.W. & NIE, S. 2005 *In vivo* molecular and cellular imaging with quantum dots. *Curr. Opin. Biotech.* **16** (1), 63–72.

GUAZZELLI, E. & MORRIS, J.F. 2011 *A Physical Introduction to Suspension Dynamics*, vol. 45. Cambridge University Press.

HEYES, D.M. & MELROSE, J.R. 1993 Brownian dynamics simulations of model hard-sphere suspensions. *J. Non-Newtonian Fluid Mech.* **46** (1), 1–28.

HUANG, Z., OMORI, T. & ISHIKAWA, T. 2020 Active droplet driven by a collective motion of enclosed microswimmers. *Phys. Rev.* E **102**, 022603.

JACKSON, L.A., *et al.* 2020 An mRNA vaccine against SARS-CoV-2 – preliminary report. *N. Engl. J. Med.* **383** (20), 1920–1931.

JONES, I.P. 1973 Low Reynolds number flow past a porous spherical shell. *Proc. Camb. Phil. Soc.* **73** (1), 231–238.

KAISER, A., PESHKOV, A., SOKOLOV, A., TEN HAGEN, B., LÖWEN, H. & ARANSON, I.S. 2014 Transport powered by bacterial turbulence. *Phys. Rev. Lett.* **112**, 158101.

LEAL, L.G. 2007 *Advanced Transport Phenomena: Fluid Mechanics and Convective Transport Processes*, vol. 7. Cambridge University Press.

LEBEDEV, V.V., TURITSYN, K.S. & VERGELES, S.S. 2007 Dynamics of nearly spherical vesicles in an external flow. *Phys. Rev. Lett.* **99**, 218101.

LIGHTHILL, M.J. 1952 On the squirming motion of nearly spherical deformable bodies through liquids at very small Reynolds numbers. *Commun. Pure Appl. Maths* **5** (2), 109–118.

MARCHETTI, M.C., JOANNY, J.F., RAMASWAMY, S., LIVERPOOL, T.B., PROST, J., RAO, M. & SIMHA, R.A. 2013 Hydrodynamics of soft active matter. *Rev. Mod. Phys.* **85**, 1143–1189.

MARSHALL, K.J. & BRADY, J.F. 2021 The hydrodynamics of an active squirming particle inside of a porous container. *J. Fluid Mech.* **919**, A31.

MASOUD, H. & STONE, H.A. 2019 The reciprocal theorem in fluid dynamics and transport phenomena. *J. Fluid Mech.* **879**, P1.

MEDINA-SÁNCHEZ, M., XU, H. & SCHMIDT, O.G. 2018 Micro- and nano-motors: the new generation of drug carriers. *Ther. Deliv.* **9** (4), 303–316.

PARK, B.-W., ZHUANG, J., YASA, O. & SITTI, M. 2017 Multifunctional bacteria-driven microswimmers for targeted active drug delivery. *ACS Nano* **11** (9), 8910–8923.

PATTNI, B.S., CHUPIN, V.V. & TORCHILIN, V.P. 2015 New developments in liposomal drug delivery. *Chem. Rev.* **115** (19), 10938–10966.

PENG, Z. & BRADY, J.F. 2020 Upstream swimming and Taylor dispersion of active Brownian particles. *Phys. Rev. Fluids* **5**, 073102.

RAO, J., DRAGULESCU-ANDRASI, A. & YAO, H. 2007 Fluorescence imaging *in vivo*: recent advances. *Curr. Opin. Biotech.* **18** (1), 17–25.

ROW, H. & BRADY, J.F. 2020 Reverse osmotic effect in active matter. *Phys. Rev.* E **101**, 062604.

SAFFMAN, P.G. 1971 On the boundary condition at the surface of a porous medium. *Stud. Appl. Maths* **50** (2), 93–101.

SAINTILLAN, D. & SHELLEY, M.J. 2015 *Theory of Active Suspensions*, 319–355. Springer.

SCHNITZER, M.J. 1993 Theory of continuum random walks and application to chemotaxis. *Phys. Rev.* E **48**, 2553–2568.

SINGH, A.V., ANSARI, M.H.D., LAUX, P. & LUCH, A. 2019 Micro-nanorobots: important considerations when developing novel drug delivery platforms. *Expert Opin. Drug Del.* **16** (11), 1259–1275.

SINGH, A.V., HOSSEINIDOUST, Z., PARK, B.-W., YASA, O. & SITTI, M. 2017 Microemulsion-based soft bacteria-driven microswimmers for active cargo delivery. *ACS Nano* **11** (10), 9759–9769.

SOKOLOV, A., APODACA, M.M., GRZYBOWSKI, B.A. & ARANSON, I.S. 2010 Swimming bacteria power microscopic gears. *Proc. Natl Acad. Sci. USA* **107** (3), 969–974.

SPAGNOLIE, S.E. & LAUGA, E. 2010 Jet propulsion without inertia. *Phys. Fluids* **22** (8), 081902.

STONE, H.A. & SAMUEL, A.D.T. 1996 Propulsion of microorganisms by surface distortions. *Phys. Rev. Lett.* **77**, 4102–4104.

STROKA, K.M., JIANG, H., CHEN, S.-H., TONG, Z., WIRTZ, D., SUN, S.X. & KONSTANTOPOULOS, K. 2014 Water permeation drives tumor cell migration in confined microenvironments. *Cell* **157** (3), 611–623.

TAILLEUR, J. & CATES, M.E. 2008 Statistical mechanics of interacting run-and-tumble bacteria. *Phys. Rev. Lett.* **100**, 218103.

TAKATORI, S.C. & BRADY, J.F. 2014 Swim stress, motion, and deformation of active matter: effect of an external field. *Soft Matt.* **10**, 9433–9445.

TAKATORI, S.C., DE DIER, R., VERMANT, J. & BRADY, J.F. 2016 Acoustic trapping of active matter. *Nat. Commun.* **7** (1), 10694.

TAKATORI, S.C. & SAHU, A. 2020 Active contact forces drive nonequilibrium fluctuations in membrane vesicles. *Phys. Rev. Lett.* **124**, 158102.

TAKATORI, S.C., YAN, W. & BRADY, J.F. 2014 Swim pressure: stress generation in active matter. *Phys. Rev. Lett.* **113**, 028103.

TORCHILIN, V.P. 2012 Multifunctional nanocarriers. *Adv. Drug Deliver. Rev.* **64**, 302–315.

TRANTIDOU, T., DEKKER, L., POLIZZI, K., CES, O. & ELANI, Y. 2018 Functionalizing cell-mimetic giant vesicles with encapsulated bacterial biosensors. *Interface Focus* **8** (5), 20180024.

TREFETHEN, L.N. 2000 *Spectral Methods in MATLAB*. Society for Industrial and Applied Mathematics.

VLAHOVSKA, P.M. & GRACIA, R.S. 2007 Dynamics of a viscous vesicle in linear flows. *Phys. Rev.* E **75**, 016313.

VUTUKURI, H.R., HOORE, M., ABAURREA-VELASCO, C., VAN BUREN, L., DUTTO, A., AUTH, T., FEDOSOV, D.A., GOMPPER, G. & VERMANT, J. 2020 Active particles induce large shape deformations in giant lipid vesicles. *Nature* **586** (7827), 52–56.

WEADY, S., SHELLEY, M.J. & STEIN, D.B. 2022 A fast Chebyshev method for the Bingham closure with application to active nematic suspensions. *J. Comput. Phys.* **457**, 110937.

WEST, J.L. & HALAS, N.J. 2003 Engineered nanomaterials for biophotonics applications: improving sensing, imaging, and therapeutics. *Annu. Rev. Biomed. Engng* **5** (1), 285–292.

YAN, W. & BRADY, J.F. 2015 The force on a boundary in active matter. *J. Fluid Mech.* **785**, R1.

YAN, W. & BRADY, J.F. 2018 The curved kinetic boundary layer of active matter. *Soft Matt.* **14**, 279–290.

YE, H. & CURCURU, A. 2015 Vesicle biomechanics in a time-varying magnetic field. *BMC Biophys.* **8** (1), 2.

ZAMPOGNA, G.A. & GALLAIRE, F. 2020 Effective stress jump across membranes. *J. Fluid Mech.* **892**, A9.